Kerbala Journal for Engineering Science

https://kjes.uokerbala.edu.iq

Determining numerically the Natural Frequency of Porous Functionally Graded Beam

Nadia Kareem Abood *,Luay S. Al-Ansari **

* Department of Mechanical Engineering, Collage of Engineering University of Kufa, Najaf, Iraq
E-mail: nadiak.alzobaie@student.uokufa.edu.iq

** Najaf Al-Ashraf Education Directorate / Vocational Education Department / Najaf Vocational Preparatory School
E-mail: Luays.alansari@uokufa.edu.iq

Received: 08 March 2024; Revised: 10 April 2024; Accepted: 24 June 2024

Abstract

In this work, the free vibration investigation of a porous functionally graded (FG) beam with the material properties varying along the height of the beam utilizing first-order shear-deformation theory and under (clamped-clamped, clamped-free, and simply supported) boundary conditions is studied. The power-law model describes the material properties. The materials used in a typical case of functionally graded (FG) beam consist of aluminum (AL) and Alumina (AL2O3). Two types of porosity distribution functions (even and uneven) are considered. The finite element model is applied by utilizing the ANSYS APDL version 17.2 and using element "SHELL281 to calculate the natural frequencies and show the influences of length-to-height ratio (L/h), power-law index (K), porosity distribution model, and porosity index (α). The numerical results are compared with some previous studies to check the accuracy of the present model, which shows a good agreement. Also, the new numerical results are used to investigate the effects of the porosity distribution function, power-law index, porosity index, and support types for the FG beam's first three non-dimensional frequency parameters. As the power-law index rises (K), the first three frequency parameters for even porous FG beams decrease, while increasing the porosity index decreases the frequency parameter. The impact of the power-law index and porosity index is observed in Uneven porous FG beams due to the porosity distribution in the cross-section area of the FG beam. The length-to-height ratio has minimal influence. Frequency parameters increase with higher mode numbers.

Keywords Porous Beam, Natural Frequency, Functionally Graded Beam, Power Law Model, ANSYS Software, Finite Element Method.

Notation

$E(z)$	Modulus of elasticity at any point in height of FG beam.
$\mu(z)$	Poisson ratio at any point in height of FG beam.
$\rho(z)$	Density at any point in height of FG beam.
E_{top}	Modulus of elasticity of top material
E_{bottom}	Modulus of elasticity of bottom material
$g(z)$	Function described of porosity distribution in cross section area of porous beam
α	Porosity index
k	Power law index

1. Introduction.

Composite materials are one of the modern materials created to develop the material properties to achieve the requirements of modern engineering applications. The physical combination of two or more materials is the basic idea of composite material. Several methods can be used to achieve this combination and to get better material properties. One of these methods is the combination of different materials as layered media (called laminated composite materials). This type of combination leads to the occurrence of stress and temperature discontinuities in the material. [1]. In 1980, Functionally graded materials were a novel kind of material. (FGM) were suggested to overcome this problem. The properties of these materials undergo a progressive transformation from one material to another based on a specified function. Nowadays, due to their excellent properties, FG materials are widely used in many fields, especially in aerospace, nuclear, biomedical, and optical engineering applications [2-5]. Numerous studies on the mechanical behavior of structures have been done as a result of the widespread use of FGM [6-13]. However, during the manufacturing process, these materials may display certain flaws like porosity. Therefore, a study on this topic has to be added as soon as possible to have a solid understanding of the porosity effect on the mechanical behavior of FGM. Because of its various applications, beams—along with plates and shells—have always piqued the interest of researchers among the three types of structures. Simple beam theory, classical beam theory, and higher-order shear deformation theory are just a few of the many beam theories that are used to analyze beam structures. On the other hand, researchers can lower the computational expense and keep the consequent error within the permitted range by employing a straightforward model. Furthermore, in order to give the designer an accurate understanding of the mechanical properties, beams composed of materials that are functionally graded and have existing porosity should be appropriately investigated.

Chen et al. [14] studied porous FG beams' static bending and elastic buckling depending on the Timoshenko beam theory. The material properties and porosity are gradually distributed along the thickness of the FG beam. Two distribution models are used to describe the porosity distribution. They calculated the critical buckling load and transverse bending deflection using the Ritz method with different boundary conditions to investigate the impact of porosity and slenderness ratio (L/h). Also, Wattanasakulpong and Chaikittiratana [15] analyzed the flexural vibration of beams under various boundary conditions, considering the effect of rotary inertia, shear deformation, and axial inertia and using the Timoshenko beam theory. The revised rule of mixture utilized porosity, assuming three types of porous distribution models across the beam section, to determine the material parameters of the FGM beams, such as the volume fraction. They calculated the natural frequencies of FG porous FG beams with different end conditions, and they found that "FGM beams with uniform porosity distribution have a stronger influence on natural frequencies compared to FGM beams with uneven porosity distribution. This method is effective for eigenvalue analysis of structural problems."

In 2016, Al Rjoub et al. [16] developed an analytical method to study the free vibration of porous FG beams with differing boundary conditions using Euler-Bernoulli and Timoshenko's theory. They employed the transfer matrix method in order to compute non-dimensional frequencies of pure and porous FG beams, assuming the uniform distribution of porosities across the thickness of the beam. Their results showed the effects of porosity, slenderness ratio, boundary conditions, material volume, and fraction index on non-dimensional frequencies of pure and porous FG beams. M.R. Galeban et al. [17] studied the free vibration of the porous beams by deriving the governing equations using the Euler-Bernoulli theory. The mechanical properties are changes in the cross-section porous beam. The results showed that "the porosity, mass, fluid compressibility, distribution of pores, and boundary conditions impact the natural frequencies of beams. Hinged-hinged beams exhibit unique natural frequency behavior".

Fouda et al. [18] investigated the effect of porosity on the mechanical behavior of the FG beam, assuming the Euler-Bernoulli beam and power distribution along the thickness of the FG beam to construct the governing equations and the kinematic relations. They concluded that "the static deflection and buckling load affected the porosity and the material distribution parameter, while the material exponent influences the frequency and has a stronger correlation with porosity in the proposed model." Akbaş [19] investigated the forced vibrations of porous FG deep beams subjected to dynamic loading. In deep beams, the mechanical properties vary along the thickness direction due to the presence of

porosity. Hamilton procedure was used to solve the problems of the governing equations. The finite element method is utilized to resolve the problems within the plane solid continua model. Amir et al. [20] analyzed the vibration behavior of a sandwich micro-beam composed of a porous core and face sheets reinforced with FG carbon nanotubes and supported on a Winkler-Pasternak substrate. In their analysis, they considered the beam's response to thermal load and employed sinusoidal shear deformation beam theory to describe the displacement components, assuming that the properties of the core and facial sheets are dispersed throughout their height. They applied Hamilton's principle and Navier's method to drive the equations of motion to study the influence of porosity coefficient and distributions, small scale, different types of CNTs distribution, and geometrical size of the beam. The study findings indicate that the frequency decreases when the porosity increases.

In 2020, Zanoosi [21] studied a vibration analysis of a porous FG micro-beam while considering the influence of thermal effects by utilizing the elasticity of modified strain gradient theory (MSGT). They used MSGT instead of MCST to analyze the size-dependent porous structures, and they applied Hamilton's principle and the Navier solution to determine the natural frequency of the micro-beam under simply supported conditions. They studied the effect of length scale, temperature changes, gradient index, slender ratio, and porosity volume fraction on FG micro-beam natural frequency. They concluded that the temperature increases reduced the micro-beam's natural frequency.

Zghal et al. [22] applied a refined mixed finite element beam model for studying static bending analysis of porous FG beams. They used two distributions of porosity (even and uneven), and to ascertain the material properties of porous FG beams, they used a modified power law model. They conducted a parametric study to examine how the boundary conditions, porosity coefficient, types of porosity distributions, and power law index affect the FG beams' deflections and stresses. They concluded that "the porosity parameter in the construction of modern buildings cannot be overstated. The proportion of porosity present in the structure can profoundly impact its overall performance and response".

Rahmani et al. [23] used different beam theories to study bending, buckling, and porous and FG beams' free vibration. They employed the finite element approach to solve problems assuming a power law model to represent the material properties along the height of the FG beam, and they used Hamilton's principle to drive the equation of motion. They investigated the impact of porosity exponents, power-law index, and boundary condition on the bending behavior, buckling characteristics, and natural frequencies of the beam using ANSYS Software. They found that natural frequencies, critical buckling load, and deflection increase when the slenderness ratio (L/h) increases. Also, the non-dimensional

frequencies decrease with decreasing values of the porosity index and power law. Ultimately, the FG beam becomes less rigid as porosity and power-law index increase, leading to higher deflection and decreased critical buckling load".

Karamanli and Vo [24] used three alternative models of porosity distribution to examine the size-dependent behavior of porous FG micro-beams utilizing a modified strain gradient theory and a quasi-3D theory. They applied the rule of mixture to determining material properties and material length scale parameters (MLSPs) based on the porosity coefficient, thickness, and gradient index, thereby enabling a comprehensive understanding of the material characteristics. They checked the accuracy of the proposed model and studied the effects of varying MLSP, gradient index, porosity coefficient, and boundary condition on responses of FG porous micro-beam.

Rahmani [25] modified the high-order sandwich beam theory to study the frequency responses of clamped-free sandwich beams with homogeneous face sheets and a FG core using a modified power-law model and two porosity distribution models to characterize the material qualities along its height. They applied Hamilton's principle and a Galerkin method to solve Governing equations of motion. They showed a comparison with specific scenarios outlined in existing literature. They concluded that "as a power-law index, temperature, cross-section, length, and porosity volume fraction increase, the basic frequency parameter falls. Conversely, an increase in the wave number leads to an increase in the frequency".

Anirudh et al. [26] used a trigonometric shear deformation theory to examine the bending vibration and buckling behavior of curved beams composed of porous FG graphene-reinforced nanocomposites to study the impact of different theories on static and dynamic performance. They used Lagrangian equations of motion and finite element analysis to derive the governing equilibrium equations. They conducted a comprehensive study to assess how parameters such as radius of curvature, porosity coefficient, length-to-thickness ratio, distribution pattern of porosity and graphene platelets, platelet geometry, and boundary conditions affect static bending, elastic stability, and free vibration.

To [5] studied the impact of porosity on the free vibration behavior of a porous FG beam using simple beam theory. He examined the effects of boundary conditions, porosity distribution models, and power-law index on the free vibration behavior of the porous FG beam. He concluded that "the results align well with existing references and confirm the applicability of classical beam theory in analyzing functionally graded porous beams. The mechanical information provided may prove useful to designers for specific purposes".

Adıyaman [1] analyzed the porous FG beam's free vibration behavior utilizing a higher-order shear deformation theory. He used Lagrange's principle, power law model, and different porosity distribution functions to derive the governing equations and applied the finite element method to solve these equations. He calculated the dimensionless natural frequencies and studied the influence of material properties, boundary conditions, and porosity on the dimensionless neutral frequencies and mode shapes. His results showed that "The mode shapes have comparable traits. despite the influence of porosity on frequencies".

Nguyen et al. [27] investigated three models of porosity distribution using a straightforward two-variable shear deformation theory to examine the vibration, bucking, and bending characteristics of porous FG beams. They used Lagrange's principle, the power law model, to derive the governing equations. They employed exponential approximations to determine the buckling load, deflection., frequency, and. stress of beams under various boundary conditions using the ANSYS model. They studied the influence of boundary conditions, porosity parameters, porous distribution pattern, height-to-span ratio, and shear deformation on the stress., deflection., frequency., and critical buckling load of beams.

Turan et al. [28] analyzed the buckling behavior and porous FG beam's unrestricted vibration under different boundary conditions considering first-order shear deformation theory. They applied the power law model, Lagrange's principle, and the Ritz method to derive and solve the equations of motion analytically. At the same time, they used finite element (FEM) and artificial neural network (ANN) methods to solve the problem numerically. They investigated the critical buckling loads and normalized fundamental frequencies for different boundary conditions, porosity coefficient, power-law index, slenderness (L/h), and porosity distribution models. The results obtained from the analytical, FEM, and ANN methods were found to be in good agreement.

In this work, the finite element model is built using ANSYS APDL to calculate the free vibration problem of porous FG beam and investigated the impacts of porosity, power law index, length-to-height ratio and supporting types on the natural frequencies and shape mode with different supporting types (Clamped-Clamped, Clamped-Free and Simply Supported).

2. Problem Description.

Changes in the FG's mechanical and physical characteristics beam along its height are necessary for a number of structural and mechanical applications. Three widely used models were used to

characterize this difference in material properties over the height of the FG beam: The sigmoid, exponential, and power-law models. A FG beam with dimensions of length (L), height (h), and width (W) is examined in this work, as shown in Figure (1). The variation of Poisson ratio, modulus of elasticity, and density along the height of the FG beam can described as the following equations using the power-law model [29,30]:

$$E(z) = \left(E_{top} - E_{bottom}\right)\left(0.5 + \frac{z}{h}\right)^{k} + E_{bottom} \quad (1\text{-a})$$

$$\mu(z) = \left(\mu_{top} - \mu_{bottom}\right)\left(0.5 + \frac{z}{h}\right)^{k} + \mu_{bottom} \quad (1\text{-b})$$

$$\rho(z) = \left(\rho_{top} - \rho_{bottom}\right)\left(0.5 + \frac{z}{h}\right)^{k} + \rho_{bottom} \quad (1\text{-c})$$

Where:

$E(z)$, $\mu(z)$and $\rho(z)$ are the modulus of elasticity, Poisson ratio, and density at any point in the height of the FG beam. E_{top} and E_{bottom} are the modulus of elasticity of top and bottom materials. μ_{top} and μ_{bottom} are Poisson ratio of top and bottom materials. ρ_{top} and ρ_{bottom} are the density of top and bottom materials. *k* is a power-law index or material distribution index (h) is the height of the FG beam and (z) is coordinated along the height of the FG beam (see Fig. (1)).

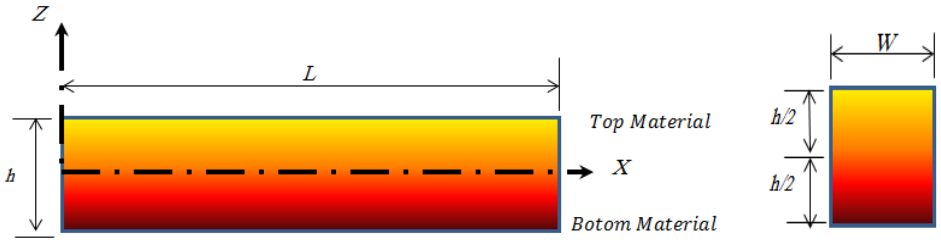

Figure 1. The Geometry of FG Beam.

Two materials that are frequently utilized in the creation of FG materials are ceramics and metal. But during the fabrication process, voids and cavities (which are typically created in contrast to the metallic phase, in the ceramic phase) form in the FG materials. Researchers have been concentrating on figuring out how this porosity affects the FG beam's mechanical behavior lately. Several researchers assumed.

The material qualities are generally impacted by the porosity in the beam and can described as:

$$E(z) = \left(E_{top} - E_{bottom}\right)\left(0.5 + \frac{z}{h}\right)^{k} + E_{bottom} - \left(\frac{\alpha}{2}\right) * g(z) * \left(E_{top} + E_{bottom}\right) \quad (2\text{-a})$$

$$\mu(z) = (\mu_{top} - \mu_{bottom})\left(0.5 + \frac{z}{h}\right)^{k} + \mu_{bottom} - \left(\frac{\alpha}{2}\right) * g(z) * (\mu_{top} + \mu_{bottom}) \quad (2\text{-b})$$

$$\rho(z) = (\rho_{top} - \rho_{bottom})\left(0.5 + \frac{z}{h}\right)^{k} + \rho_{bottom} - \left(\frac{\alpha}{2}\right) * g(z) * (\rho_{top} + \rho_{bottom}) \quad (2\text{-c})$$

Where: α is the porosity index (0<α<1) and $g(z)$ is the function described by the porosity distribution in the cross section area of the porous beam. In this study, two kinds of porosity distribution (even and uneven) are considered, as seen in Figure (2), and these porosity distributions can describe by the following equations:

$$g_1(z) = 1 \quad (3\text{-a})$$

$$g_2(z) = Sin\left(\frac{\pi|z|}{h}\right) \quad (3\text{-b})$$

Fig. (2) shows the porosity distribution throughout the height corresponding to the Even and Uneven distribution functions. While porosities are primarily distributed in the uneven cross-section's corners, they are uniformly distributed throughout the beam cross-section for Even. Fig. (3) displays the variation of Young's modulus ratio (E(z)/Etop) in even and uneven for distinct porosity index (α) and power-law index (K) values.

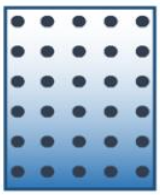

(a) Even ($g_1(z) = 1$).

(b) Uneven ($g_2(z) = \text{Sin}\left(\frac{\pi|z|}{h}\right)$)

Figure 2. The Porous Beam Cross-Sections for Tow distribution functions of Porosity Distribution (a) Even (b) Uneven [1].

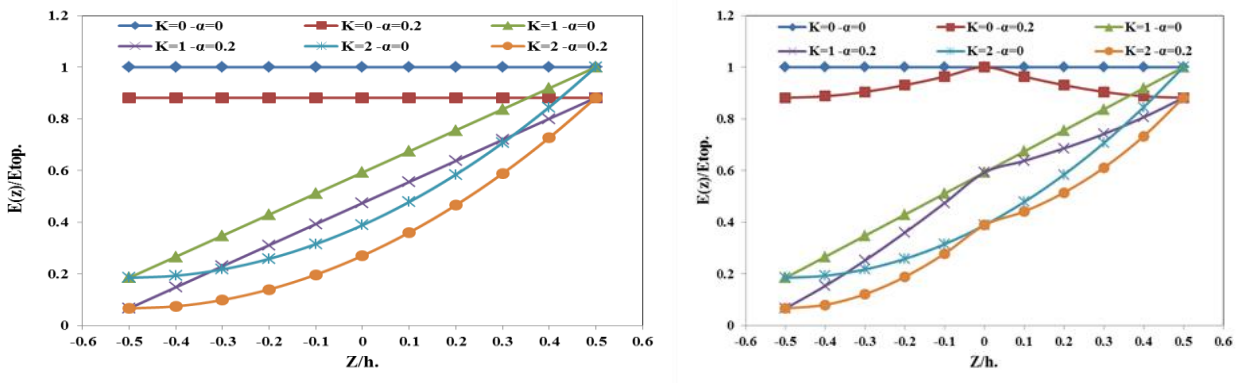

Even Uneven

Figure 3. Young's Modulus Ratio (E(z)/Etop) in Even, and Uneven When (K=0 ,1 and 2) and (α=0 and 0.2).

2. ANSYS Model

In this work, the finite element method is applied by utilizing ANSYS APDL software. The ANSYS model used the element "SHELL281" in order to vary the material properties along the height of the FG beam. The characteristics of "SHELL281" are: "Analysis of thin to moderately-thick shell structures is appropriate for SHELL281. The element consists of eight nodes, each of which has six degrees of freedom: x, y, and z-axis translations, as well as rotations around those axes. The element only has translational degrees of freedom when the membrane option is utilized. Applications requiring large rotation, large strain, or both are ideally suited for SHELL281. Nonlinear analyses take into consideration changes in shell thickness. The element takes into consideration the impact of scattered stresses on followers (load stiffness). Layered applications such as sandwich building or composite shell modeling can make use of SHELL281. First-order shear-deformation theory (also known as Mindlin-Reissner shell theory) controls modeling accuracy for composite shells. True stress measures and logarithmic strain serve as the foundation for the element formulation. Finite membrane strains are possible due to the element's kinematics (stretching). On the other hand, it is believed that the curvature variations within a time increment are minimal." [31] (see Fig. (4)).

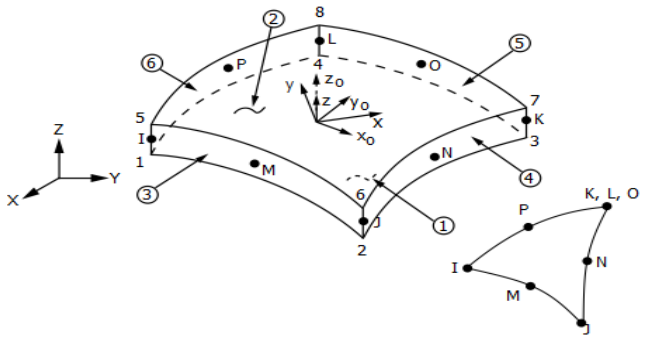

Figure 4. Geometry of SHELL281[31].

The ANSYS model of porous FG beam was built by applying the following steps [29,30]:

1. The beam is drawn as the top area of the beam (L*W), as seen in Fig. (5-a).
2. The required material properties of porous FG beam are calculated utilizing the following points:
   (a) The height of the beam is divided into (N) parts (in this work N=10). Each part is called a "layer".
   (b) The height of each layer is calculated as (height of layer= height of beam/N).
   (c) From step (a), the required material properties are calculated for (N+1) points along the height of porous FG beam using equations (2) and assuming [z_i =zo+ ((h/N) *(i-1))] where zo=-h/2 and (i) is a number of points ($1 \leq i \leq (N+1)$).
   (d) The following formula is used to determine the necessary material qualities for each layer:

$$\left(E_{layer}\right)_i = \frac{E(z_i)+E(z_{i+1})}{2} \quad (4\text{-a})$$

$$\left(\mu_{layer}\right)_i = \frac{\mu(z_i)+\mu(z_{i+1})}{2} \quad (4\text{-b})$$

$$\left(\rho_{layer}\right)_i = \frac{\rho(z_i)+\rho(z_{i+1})}{2} \quad (4\text{-c})$$

3. The (N) set of material properties is input into the ANSYS APDL software using the command "section," assuming the layer is isotropic material, as shown in Fig. (5-b).
4. The drawing area is carefully meshed using the 'SHELL281' element, with a thorough consideration of the convergence criteria of element size, as seen in Fig. (6).

5. Three types of supports are considered in this work, clamped-clamped beam (C-C), simply supported beam (S-S) and clamped-free beam (C-F). The boundary conditions of each type of support are:
   (a) Clamped-Clamped beam (C-C): All degrees of freedom (UX , UY , UZ , ROTX , ROTY, and ROTZ) of the nodes at edges x=0 and x=L are zero.
   (b) Simply Supported beam (S-S): The degree of freedom (UX , UY, and UZ) of the nodes at edge x=0 are zero. Also, the degree of freedom (UY and UZ) of the nodes at edge x=L is zero.
   (c) Clamped-Free beam (C-F): All degrees of freedom (UX, UY, UZ, ROTX, ROTY, and ROTZ) of the nodes at edge x=0 only are zero.
6. The model analysis is selected to analyze the free vibration problem of porous FG beams.

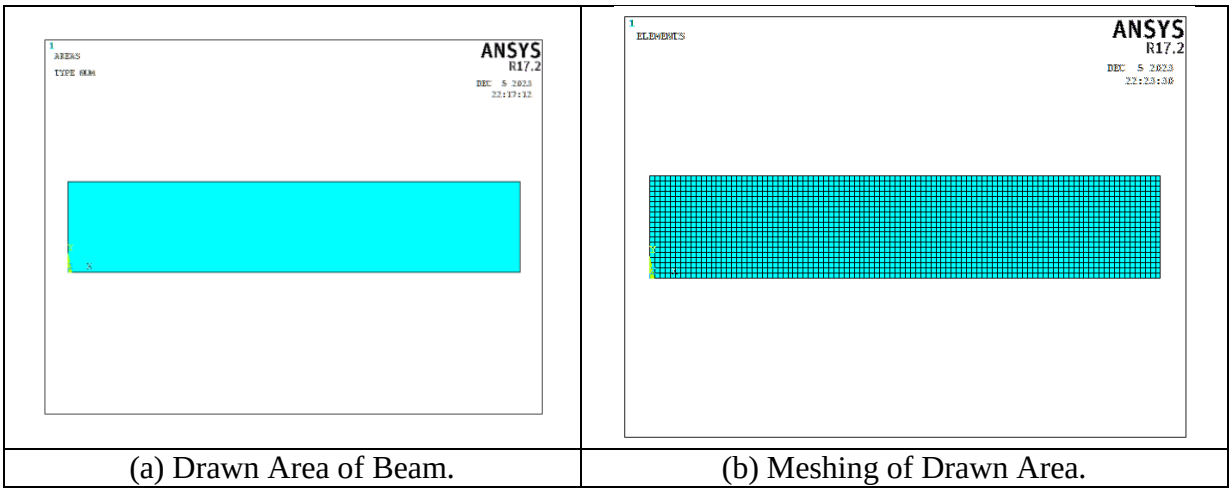

(a) Drawn Area of Beam. (b) Meshing of Drawn Area.

Figure 5. General Steps of Present ANSYS Model.

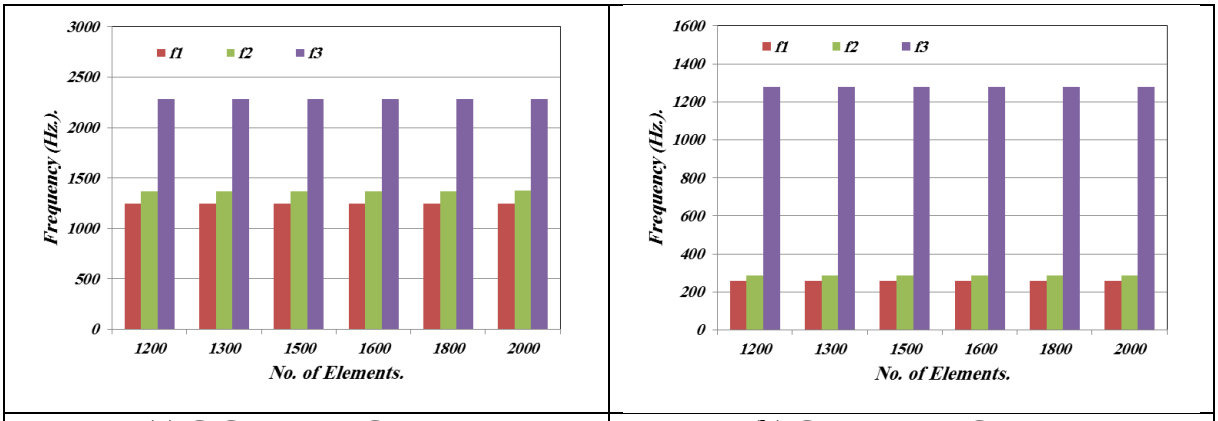

(a) C-C Porous FG Beam When α=0.2 and K=1 .	(b) C-F Porous FG Beam When α=0.3 and K=0.5.

Figure 6. Convergence Criteria of Element Size for the First Three Natural Frequencies.

3. Validation of ANSYS Model

The comparisons were made between the natural frequency results of the present model and those found in the available literature to verify the ANSYS model employed in this work. In this comparison, the FG beam consists of two materials (aluminum and Alumina), and these materials' mechanical and physical properties are listed in Table (1).

Table (1): The Material Properties of Aluminum and Alumina [4].

Material	Modulus of Elasticity (GPa)	Density (Kg/m^3)	Poisson Ratio
Aluminum	70	2707	0.3
Alumina	380	3960	0.3

The first comparison is made between the frequency results of the present model with that of Kahya and Tura [32] (utilizing the FEM approach founded on the theory of first-order shear deformation, Nguyen et al. [33] (utilized higher-order shear deformation theory as the foundation for an analytical solution technique.), Vo et al. [34] (implemented FEM with an advanced theory of shear deformation.) and Gökhan Adıyaman [1] (employed FEM with a higher-order shear deformation theory as a basis) for the perfect cross-section of power law FG beam (i.e. non-pours FG beam) (see Table (2)). Where The equation can be used to compute the dimensionless frequency parameter:

$$\bar{\omega} = \frac{\omega L^2}{h}\sqrt{\frac{\rho_m}{E_m}} \qquad (5)$$

There is a great deal of agreement in the comparison between the results of the present model and those of the available literature for non-pours FG beams with different power law indexes and different supporting types (simply supported (S-S), Clamped-clamped (C-C), and Clamped-free (C-F)).

Table (2): The Comparison Between the Frequencies Obtained in the present Work with That Reported in Kahya and Turan [32], Nguyen et al. [33], Vo et al. [34], and Gökhan Adıyaman [1] When (L/h=5).

B.C	Author	K= 0	K= 0.5	K= 1	K = 2	K = 5	K = 10
SS	Kahya and Tura [32]	5.2219	4.4692	4.0496	3.6936	3.4881	3.3643
	Nguyen et al. [33]	5.1528	4.4102	3.9904	3.6264	3.4009	3.2815
	Vo et al. [34]	5.1528	4.4019	3.9716	3.5979	3.3743	3.2653
	Gökhan Adıyaman[1]	5.1532	4.4016	3.9710	3.5970	3.3725	3.2644
	Present work	5.155718	4.370045	3.980049	3.60215	3.3654	3.26865
CF	Kahya and Tura [32]	1.9077	1.6286	1.4739	1.3446	1.2751	1.2636
	Nguyen et al. [33]	1.8957	1.6182	1.4636	1.3328	1.2594	1.2187
	Vo et al. [34]	1.8952	1.6180	1.4633	1.3326	1.2592	1.2184
	Gökhan Adıyaman[1]	1.8948	1.6176	1.4629	1.3322	1.2586	1.2178
	Present work	1.90472	1.613582	1.473539	1.340905	1.261807	1.16474
CC	Kahya and Tura [32]	10.0864	8.7547	7.9841	7.2715	6.7148	6.3741
	Nguyen et al. [33]	10.0726	8.7463	7.9518	7.1776	6.4929	6.1658
	Vo et al. [34]	10.0678	8.7457	7.9522	7.1801	6.4961	6.1662
	Gökhan Adıyaman[1]	10.0321	8.7114	7.9200	7.1496	6.4626	6.1355
	Present work	10.0660	8.70081	7.962938	7.16084	6.4396	6.10286

The second comparison is a mode to verify the authenticity of the current model of the pours FG beam. Three parameters were studied, and these parameters were power law index (0,0.5,1,2,5 and 10), porosity index (0,0.1,0.2 and 0.3), and supporting type (S-S, C-C, and C-F) in additional to the distribution function of porosity (Even and Uneven). Tables (3 and 4) compare the dimensionless frequency of the pours FGM obtained by the present model and that calculated by Adıyaman [1] when the distribution function of porosity is Even and Uneven, respectively.

For different distributions of porosity (Even and Uneven), the porous FG beam's frequency parameter results are closely matched for different porosity indexes, boundary conditions, and the power law index, and the maximum discrepancy between the comparing results does not exceed 10%. For the

Even distribution function of porosity, the maximum discrepancy between the comparing results is approximately (4.5%) for each supporting type end because the theory and its assumptions are used to solve the problem. For Uneven, the maximum discrepancy between the comparing results is (0.75, 0.5, and 4.5 %) for S-S, C-C, and C-F supports, respectively.

Table (3). The Fundamental Frequency Parameters of a Porous –FG Beam with Various Porosity Index (α), Power Law index (K) and Boundary Conditions When the Porosity Function is Even and (L/h=5).

B.C	α	Author	K = 0	K = 0.5	K= 1	K = 2	K= 5	K = 10
SS	0	Present Work	5.155718	4.370045	3.980049	3.602155	3.365477	3.268657
		Gökhan[1]	5.1532	4.4016	3.971	3.5970	3.3725	3.2644
	0.1	Present Work	5.230494	4.360659	3.897554	3.416172	3.102989	3.007281
		Gökhan[1]	5.2223	4.3934	3.8835	3.4050	3.1083	3.0028
	0.2	Present Work	5.318299	4.344111	3.777085	3.122255	2.635685	2.527751
		Gökhan[1]	5.3047	4.3798	3.7577	3.1023	2.6403	2.5273
	0.3	Present Work	5.423208	4.315892	3.591473	2.594932	1.477182	1.113058
		Gökhan[1]	5.4040	4.3573	3.5658	2.5572	1.4574	1.1164
CC	0	Present Work	10.06605	8.700818	7.962938	7.16084	6.439631	6.102861
		Gökhan[1]	10.0321	8.7114	7.9200	7.1496	6.4626	6.1355
	0.1	Present Work	10.22968	8.718108	7.85488	6.873097	5.980539	5.630864
		Gökhan[1]	10.1621	8.7170	7.7918	6.8439	6.0019	5.6231
	0.2	Present Work	10.42048	8.728605	7.686927	6.408757	5.180417	4.741579
		Gökhan[1]	10.3225	8.7178	7.6032	6.3561	5.2216	4.7437
	0.3	Present Work	10.64648	8.724282	7.409681	5.536144	3.220927	2.257545
		Gökhan[1]	10.5158	8.7094	7.3061	5.4349	3.2140	2.3636
CF	0	Present Work	1.90472	1.613582	1.473539	1.340905	1.261807	1.16474
		Gökhan[1]	1.8948	1.6176	1.4629	1.3322	1.2586	1.2178
	0.1	Present Work	1.929666	1.608086	1.441801	1.272119	1.166963	1.091014
		Gökhan[1]	1.9203	1.6147	1.4313	1.2630	1.1649	1.1266
	0.2	Present Work	1.959552	1.600121	1.39654	1.163999	0.997405	0.961283
		Gökhan[1]	1.9506	1.6098	1.3858	1.1533	0.9963	0.9592
	0.3	Present Work	1.995798	1.588203	1.327815	0.969866	0.565044	0.434232
		Gökhan[1]	1.9872	1.6016	1.3162	0.9539	0.5559	0.4339

Table (4). The Fundamental Frequency Parameters of a Pours –FG Beam with Various Porosity Index (α), Power Law index (K) and Boundary Conditions When the Porosity Function is Uneven and (L/h=5).

B.C	α	Author	K = 0	K = 0.5	K= 1	K = 2	K= 5	K = 10
SS	0	Present Work	5.155718	4.370045	3.980049	3.602155	3.365477	3.268657
		Gökhan[1]	5.1532	4.4016	3.9710	3.5970	3.3725	3.2644
	0.1	Present Work	5.169241	4.31935	3.877733	3.431423	3.151152	3.053221
		Gökhan[1]	5.1633	4.3512	3.8633	3.4184	3.1517	3.0452
	0.2	Present Work	5.183875	4.258467	3.750719	3.206787	2.850751	2.749177
		Gökhan[1]	5.1747	4.2911	3.7297	3.1828	2.8423	2.7376
	0.3	Present Work	5.199682	4.184309	3.589188	2.896506	2.389252	2.271006
		Gökhan[1]	5.1872	4.2184	3.5602	2.8568	2.3646	2.2533
CC	0	Present Work	10.06605	8.700818	7.962938	7.16084	6.439631	6.102861
		Gökhan[1]	10.0321	8.7114	7.9200	7.1496	6.4626	6.1355
	0.1	Present Work	10.12409	8.648333	7.826476	6.920642	6.142008	5.815612
		Gökhan[1]	10.0749	8.6571	7.7698	6.8867	6.1421	5.8047
	0.2	Present Work	10.18584	8.579176	7.646174	6.585354	5.703294	5.347876
		Gökhan[1]	10.1269	8.5875	7.5747	6.5227	5.6788	5.3373
	0.3	Present Work	10.25253	8.487173	7.401037	6.084892	4.972514	4.562697
		Gökhan[1]	10.1832	8.4973	7.3142	5.9865	4.9161	4.5760
CF	0	Present Work	1.90472	1.613582	1.473539	1.340905	1.261807	1.16474
		Gökhan[1]	1.8948	1.6176	1.4629	1.3322	1.2586	1.2178
	0.1	Present Work	1.906635	1.592155	1.433403	1.275577	1.180177	1.121579
		Gökhan[1]	1.8973	1.5978	1.4222	1.2654	1.1760	1.1356
	0.2	Present Work	1.908981	1.567148	1.384375	1.190736	1.067056	1.029452
		Gökhan[1]	1.9001	1.5743	1.3720	1.1777	1.0607	1.0209
	0.3	Present Work	1.911821	1.537385	1.322999	1.074898	0.89509	0.85217
		Gökhan[1]	1.9032	1.5461	1.3086	1.0569	0.8832	0.8411

4. Results and Discussion

In this study, ANSYS APDL and the element "SHELL281" are used to calculate the first three natural frequencies of a porous FG beam with three supporting types (C-C, C-F, and S-S). The effects of the supporting kinds as well as the length-to-height ratio (L/h), power-law index (K), porosity index (α), and type of porosity distribution function, are examined.

The first natural frequency results of an even porous FG beam are shown in Figure (7) for different supporting types and power-law index (K) when the porosity index (α) increases from zero to (0.3). If the power-law index (K) rises, the frequency parameter for the first natural frequency drops at any porosity index and supporting kinds. On the other hand, the influence of the porosity index varies depending on the power-law index value. For example, when the power-law index is (0), the frequency parameter grows as the porosity index increases, whereas for K=10, the frequency parameter decreases as the porosity index increases for any supporting type. However, the first frequency parameter of the C-C beam is greater than that of the S-S and C-F beams. The second and third natural frequencies exhibit a similar pattern (see Figures 8 and 9)). Additionally, the frequency parameter's value increases when the mode number increases.

To explain the above results, the frequency of Euler - Bernoulli beam is considered, as an example, and the general equation are written as [35]:

$$\omega_i = (\beta_i L)^2 * \sqrt[2]{\frac{E_{eq}*I}{\rho_{eq}*A*L^4}} \qquad i = mode\ number \tag{6}$$

The $(\beta_i L)$ value depends on the supporting type, (A) and (I) are the cross section area and second moment of area of beam and their values are constant in this work. The value of ($\sqrt[2]{\frac{E_{eq}}{\rho_{eq}}}$) is the effective part in equation (6). This part ($\sqrt[2]{\frac{E_{eq}}{\rho_{eq}}}$) depends on modulus ratio of FG beam ($\frac{E_{bottom}}{E_{top}}$), density ratio of FG beam ($\frac{\rho_{bottom}}{\rho_{top}}$) , power-law index and porosity index.

In this work, the modulus and density ratio are constant and smaller than (1) as illustrated in Table (1) (modulus ratio =$\frac{70}{380}$ and density ratio = $\frac{2707}{3960}$).According equations (1), when the power- law index is zero and infinity the equivalent material properties are the material properties of metal and ceramic respectively. When the power-law increases (larger than zero) the equivalent material will be larger than the metal material properties and smaller than the ceramic material properties. According to modulus and density ratio (modulus ratio =$\frac{70}{380}$ and density ratio =$\frac{2707}{3960}$), the equivalent modulus increases with rate larger than that of equivalent density for the same power-law index, therefor, the part ($\sqrt[2]{\frac{E_{eq}}{\rho_{eq}}}$) increases with increasing power-law index and this leads to increases frequency.

In order to investigate the impact of the porosity index, it is assumed that "the porosity in the beam averagely affects the material properties" [1]. This means the porosity is found in metal and ceramic materials simultaneously, and the impact of porosity depends on the porosity index and function of porosity distribution in addition to the average of the modulus and density of metal and ceramic (see Equations (2)). In even porous FG beams, the function of porosity distribution is constant and doesn't depend on the position in the height of the beam (i.e. (z) direction). Generally, the presence of porosity leads to decrease the material properties (modulus of elasticity and density). For pure metal beam, the reducing rate of modulus due to porosity is larger than the reducing rate of density, therefore, the part ($\sqrt[2]{\frac{E}{\rho}}$) reduces and this leads to increase the frequency of pure beam. But for pure metal beam, the reducing rate of modulus due to porosity is smaller than the reducing rate of density, therefore, the part ($\sqrt[2]{\frac{E}{\rho}}$) reduces and this leads to decrease the frequency of pure beam. For porous FG beam (i.e. $0 \leq K \leq \infty$), the increase of porosity index affects reversely on the frequency of beam while increase of the power-law index affects proportionally on the frequency of beam. In other words, the impact of power-law index is opposite to the impact of porosity index and the part ($\sqrt[2]{\frac{E_{eq}}{\rho_{eq}}}$) depends on the combination effect of these two indices.

Therefore, the part ($\sqrt[2]{\frac{E_{eq}}{\rho_{eq}}}$) decreases at high porosity index and at any power-law index. It can see that the frequency decreases when the porosity index increases at high power-law index.

Figures (10-12) show the effects of the porosity index and power-law index on the first, second, and third natural frequency parameters of porous FG beam for uneven porosity distribution function and different supporting types. From Figure (10), the first frequency parameter decreases when the porosity index increases at any power-law index and any supporting types. Also, the second and third frequency parameters decrease when the porosity index increases at any power-law index and any supporting types, as illustrated in Figures (11 and 12) respectively. Also, the frequency decreases when the porosity index increases at a high power-law index.

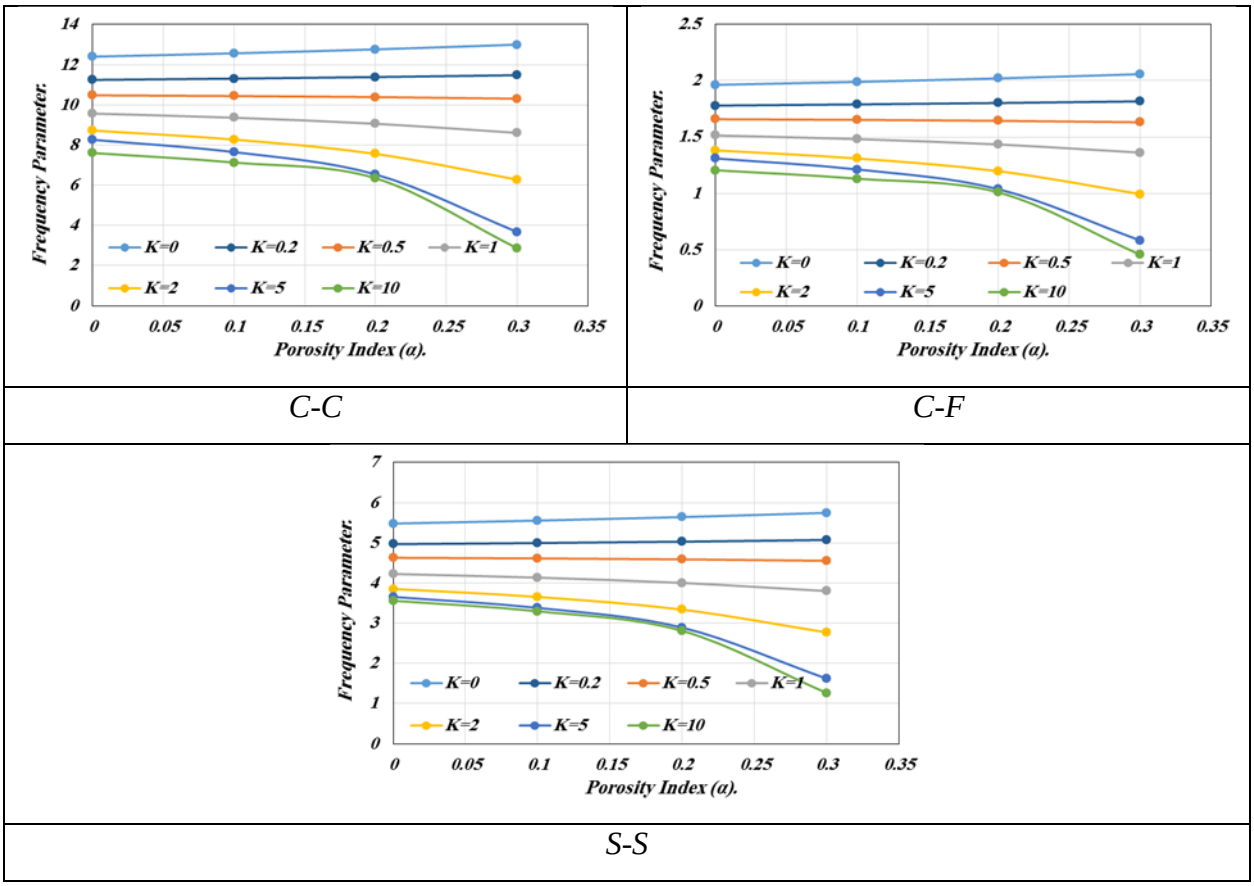

Figure 7. The Variation of the first natural frequency parameters of even porous FG beam due to variation of porosity index (α) for different supporting types when L/h=40.

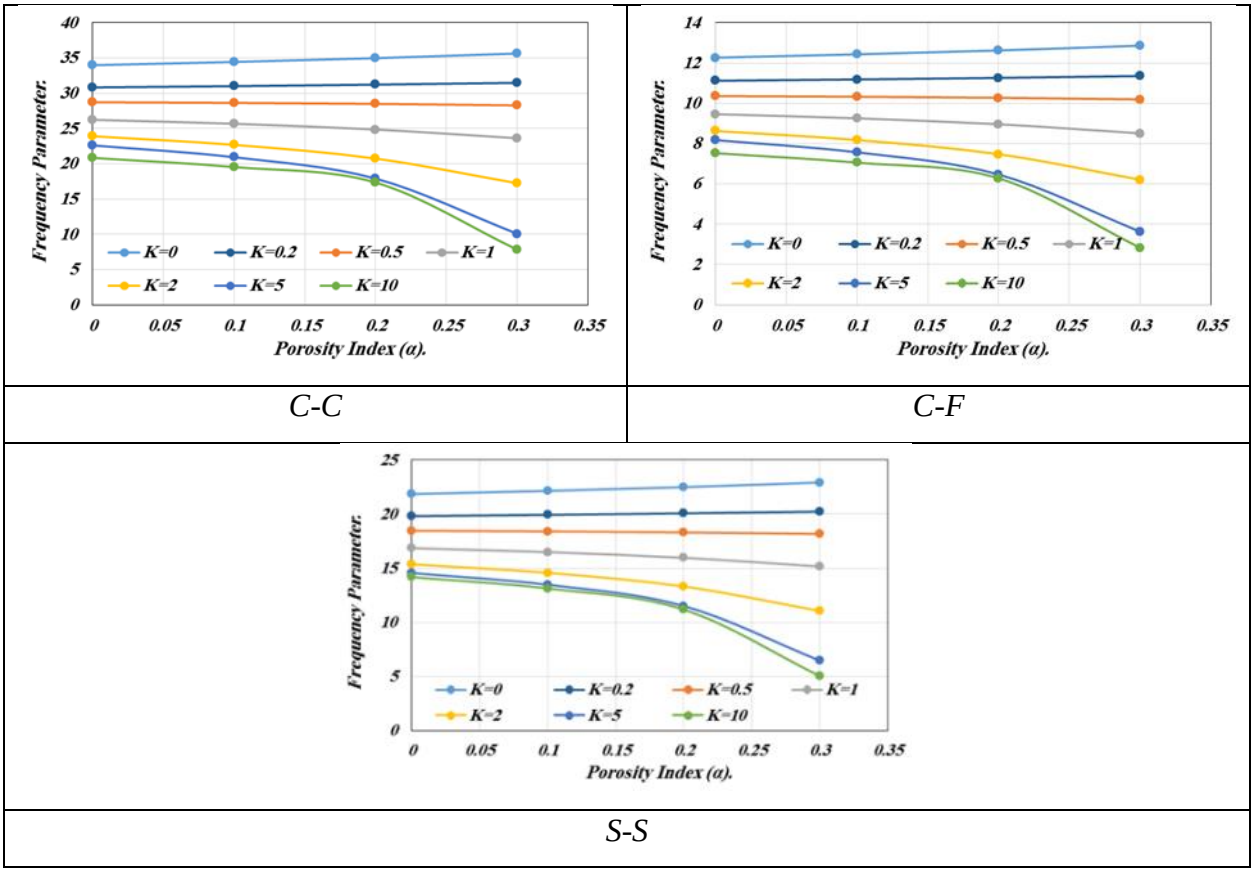

Figure 8. The Variation of the Second natural frequency parameters of even porous FG beam due to variation of porosity index (α) for different supporting types when L/h=40

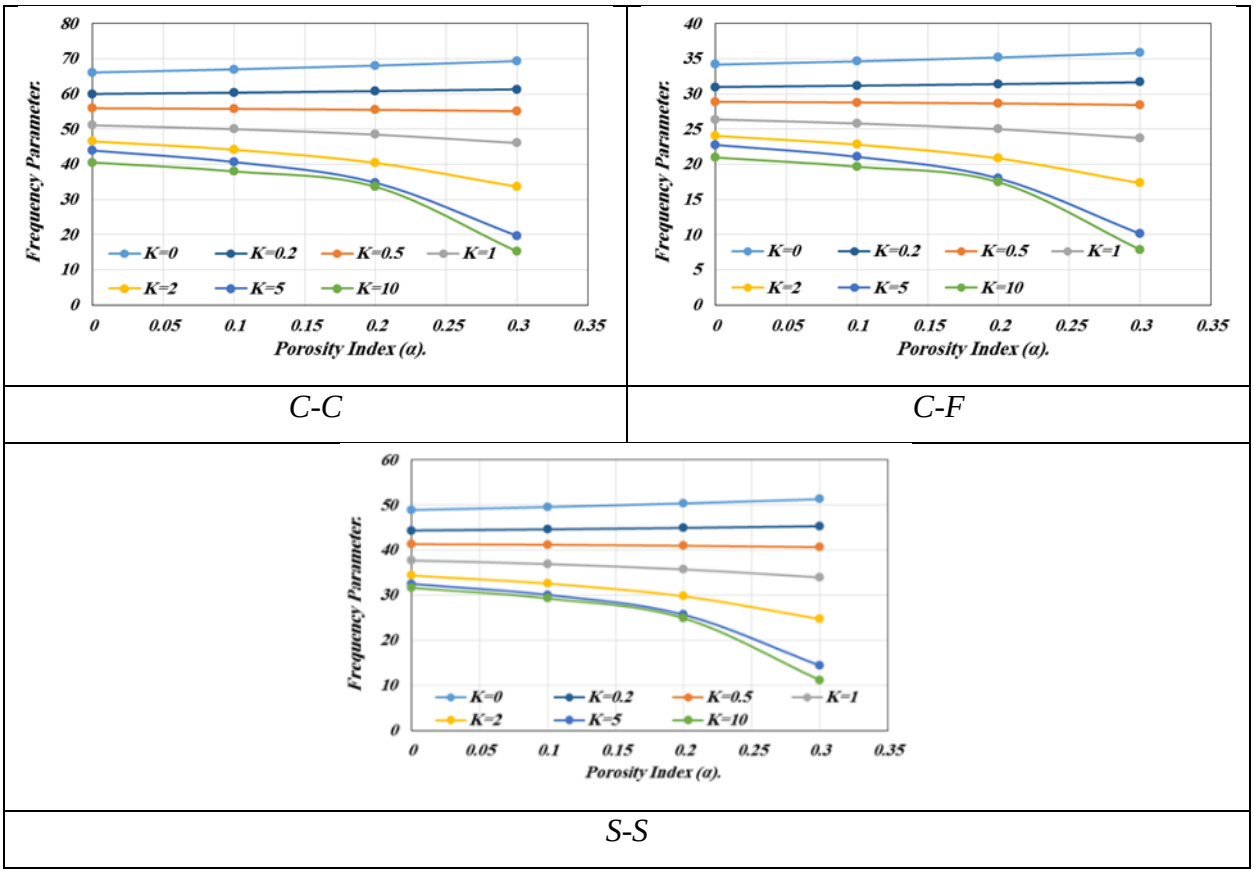

Figure 9. The Variation of the Third natural frequency parameters of even porous FG beam due to variation of porosity index (α) for different supporting types when L/h=40.

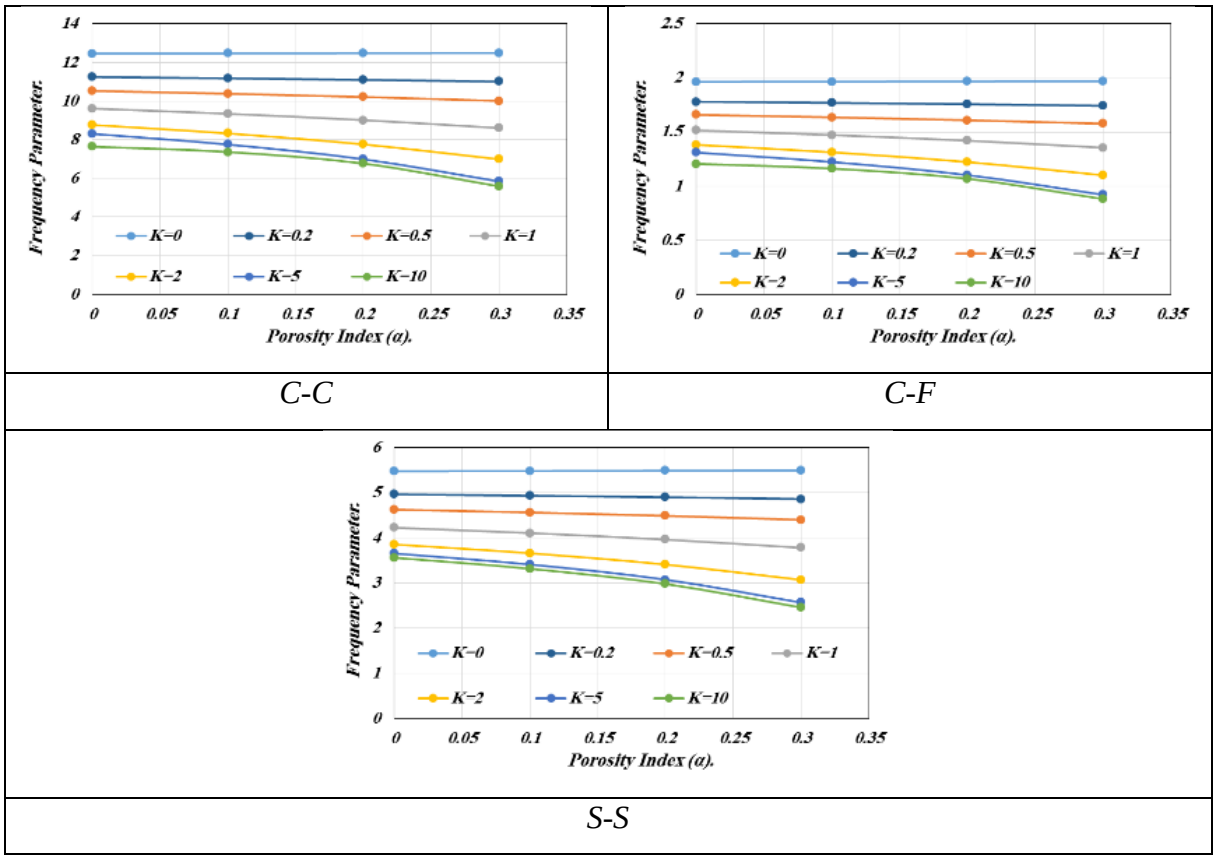

Figure 10. The Variation of the first natural frequency parameters of Uneven porous FG beam due to variation of porosity index (α) for different supporting types when L/h=40.

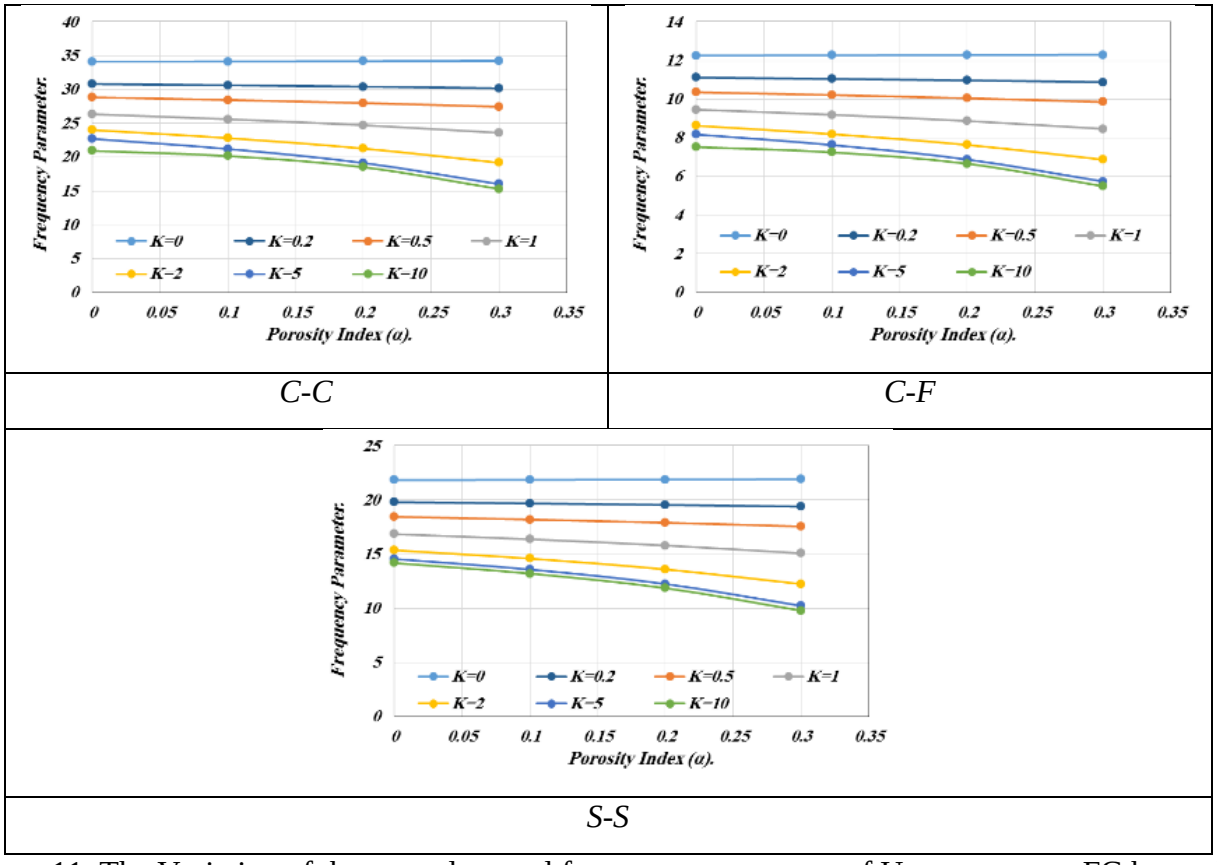

Figure 11. The Variation of the second natural frequency parameters of Uneven porous FG beam due to variation of porosity index (α) for different supporting types when L/h=40.

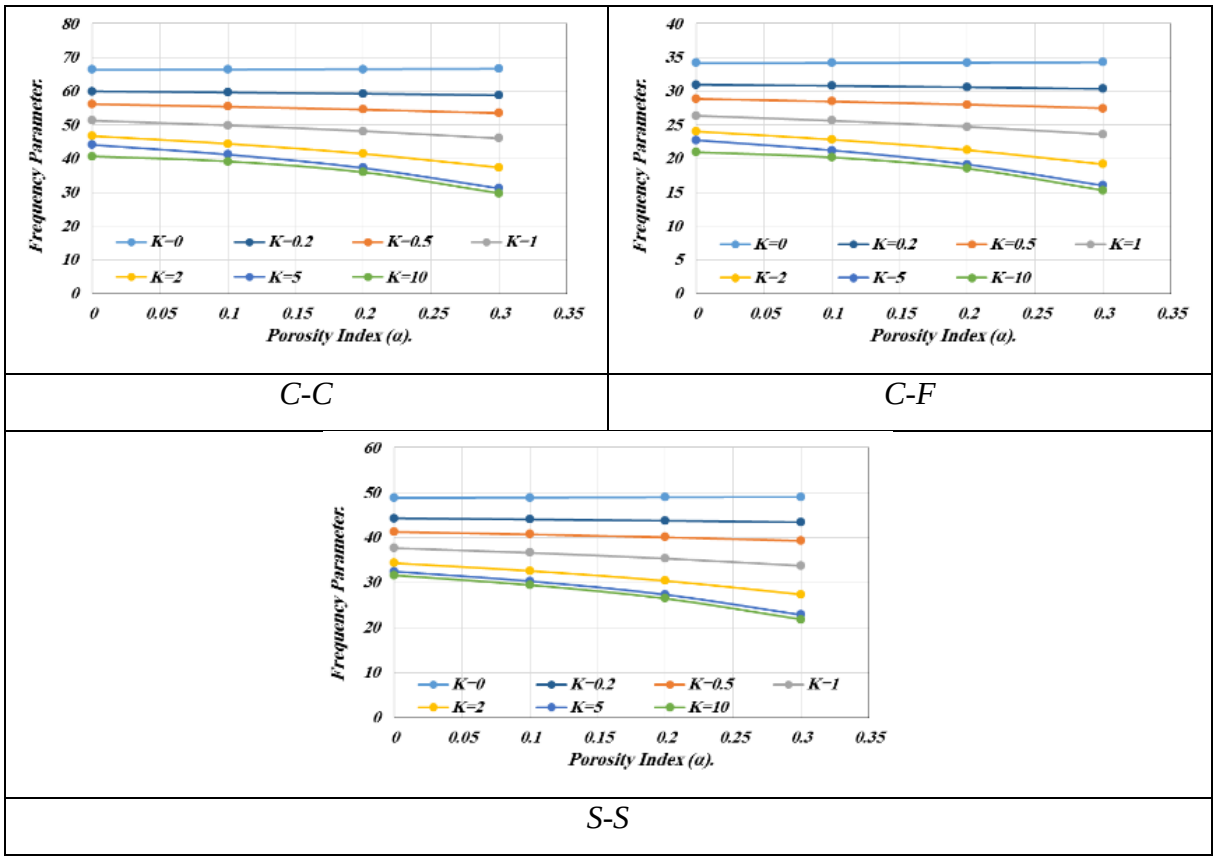

Figure 12. The Variation of the third natural frequency parameters of Uneven porous FG beam due to variation of porosity index (α) for different supporting types when L/h=40.

On the other side, Figures (13-15) show the natural frequency parameters of even porous FG beams when the power-law index (K) increases from zero to 10 for different porosity indexes and supporting types. The frequency parameter falls at every power-law index (K) as the porosity index and any supporting types rise. On the other hand, the frequency parameter of the C-C beam is more significant than that of the S-S and C-F beams (see Figure (13)). The same behavior is found in second and third natural frequencies (see Figure (14 and 15)). Also, the value of the frequency parameter increases with increasing the mode number. For the Uneven porous FG beam, the effect of the power-law index on the natural frequency parameters appears sharply. It takes the same profile in the first, second, and third natural frequencies, as illustrated in Figures (16-18). Also, the value of the frequency

parameter increases with increasing the mode number. For uneven porosity distribution function, the effect of porosity depends on (z) coordinate and concentrates at the edges of the FG beam. The impact of uneven-II porosity distribution function is smaller than that of even one. Therefore, Figure (11) shows sharply the variation in natural frequency parameters due to porosity distribution function, supporting type, and mode number.

The impact of length-to-height ratio on the first natural frequency parameter of Even and Uneven C-C FG beam for different power-law and porosity index are shown in Figure (19). The impact of the length-to-height ratio on the first natural frequency parameter of C-F and S-S porous (Even and Uneven) FG beams with different power-law and porosity index are shown in Figures (20 and 21). Generally, the effect of the length-to-height ratio on the first frequency parameter vanishes when the length-to-height ratio is more significant than (20) for any supporting type, power-law index, and porosity index. Also, the effect of the length-to-height ratio on the first frequency parameter of the C-C porous FG beam is greater than that of the S-S and C-F porous FG beam, respectively, for any power.-.law index and porosity index. The reason for this behavior is similar to that described previously. The shear effect due to variation in material properties is small when the length-to-height ratio of the porous FG beam increases. Therefore, the variation in the first frequency parameter decreases.

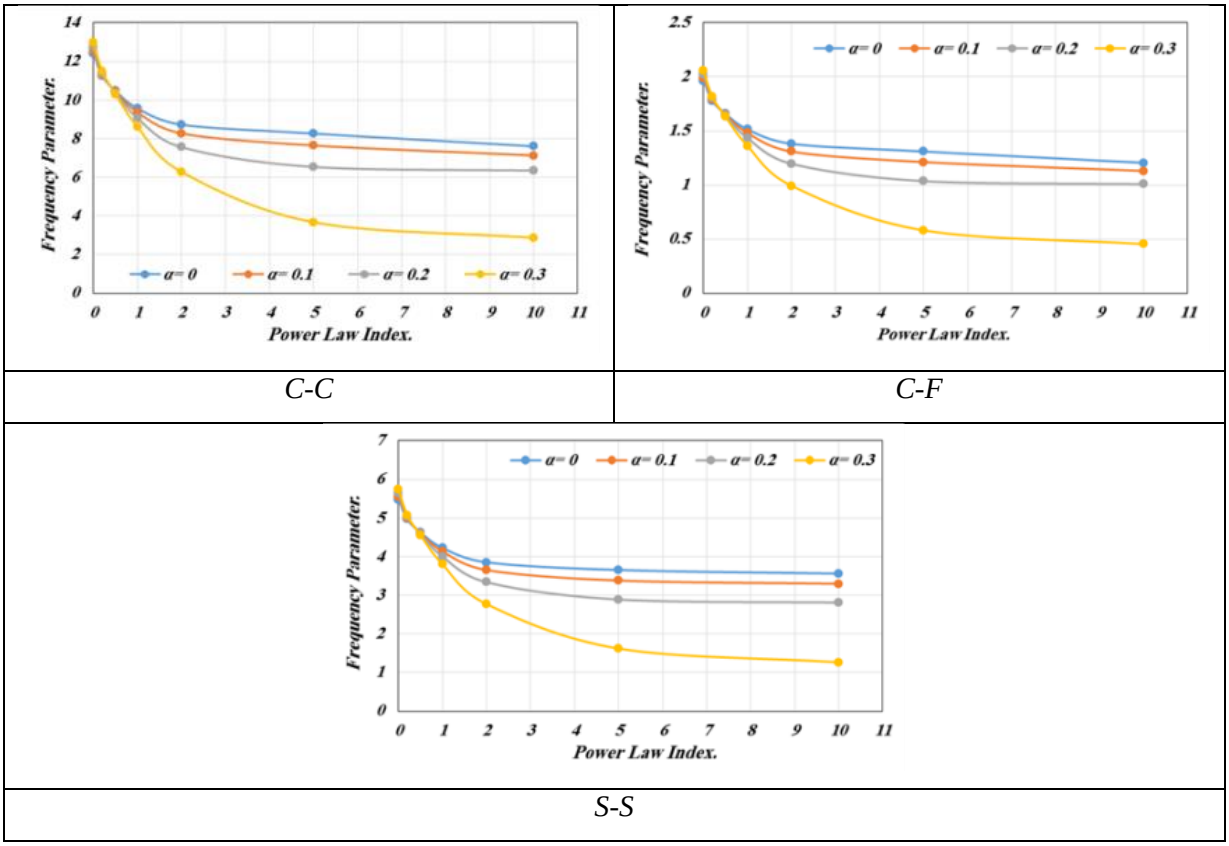

Figure 13. The Variation of the first natural frequency parameters of even porous FG beam due to variation of power-law index (K) for different supporting types when L/h=40.

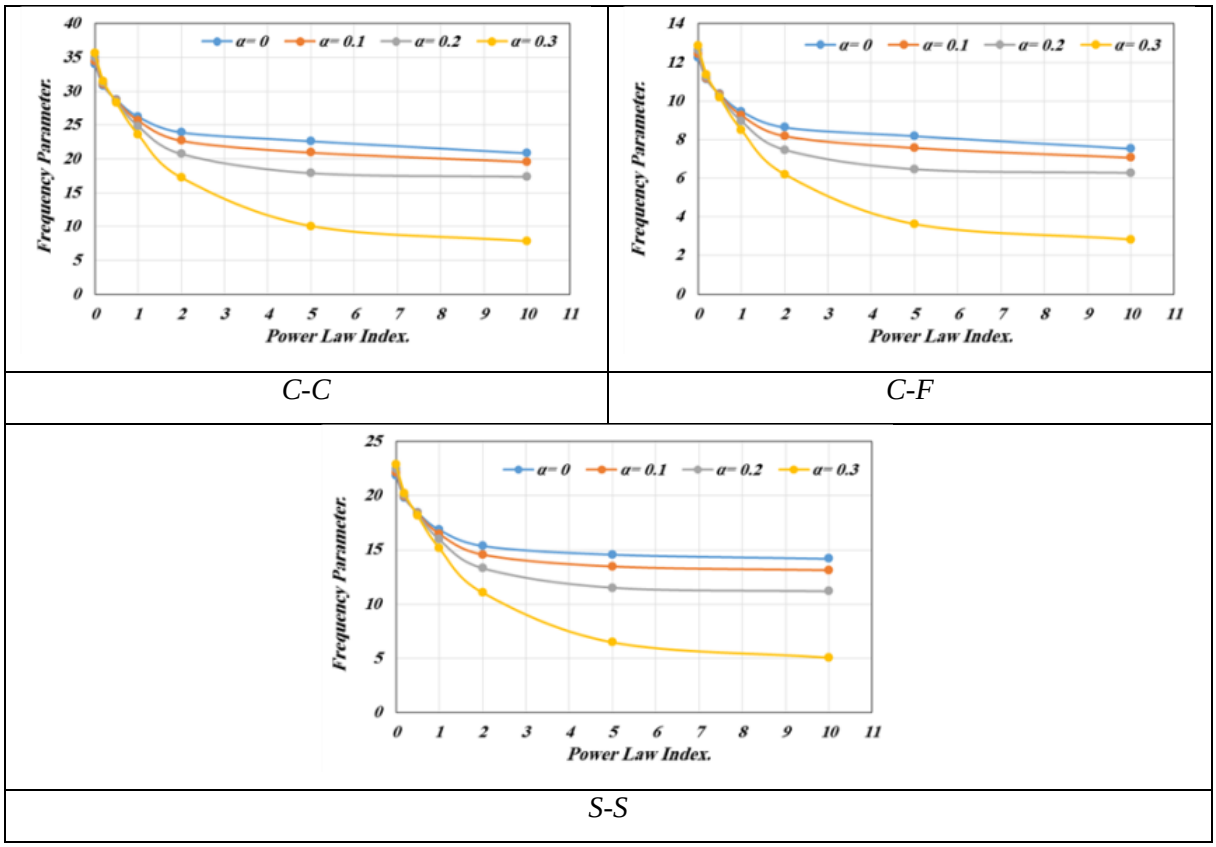

Figure 14. The Variation of the second natural frequency parameters of even porous FG beam due to variation of power-law index (K) for different supporting types when L/h=40.

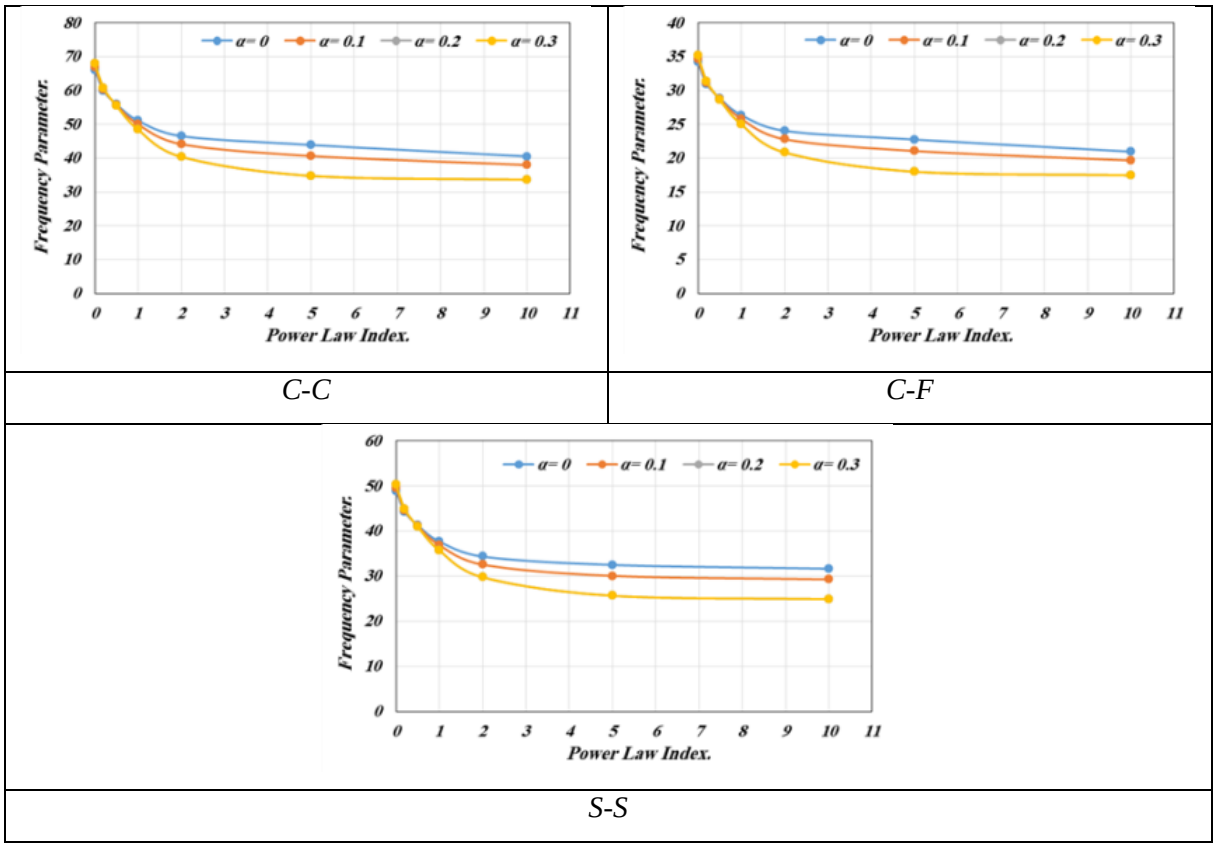

Figure 15. The Variation of the third natural frequency parameters of even porous FG beam due to variation of power-law index (K) for different supporting types when L/h=40.

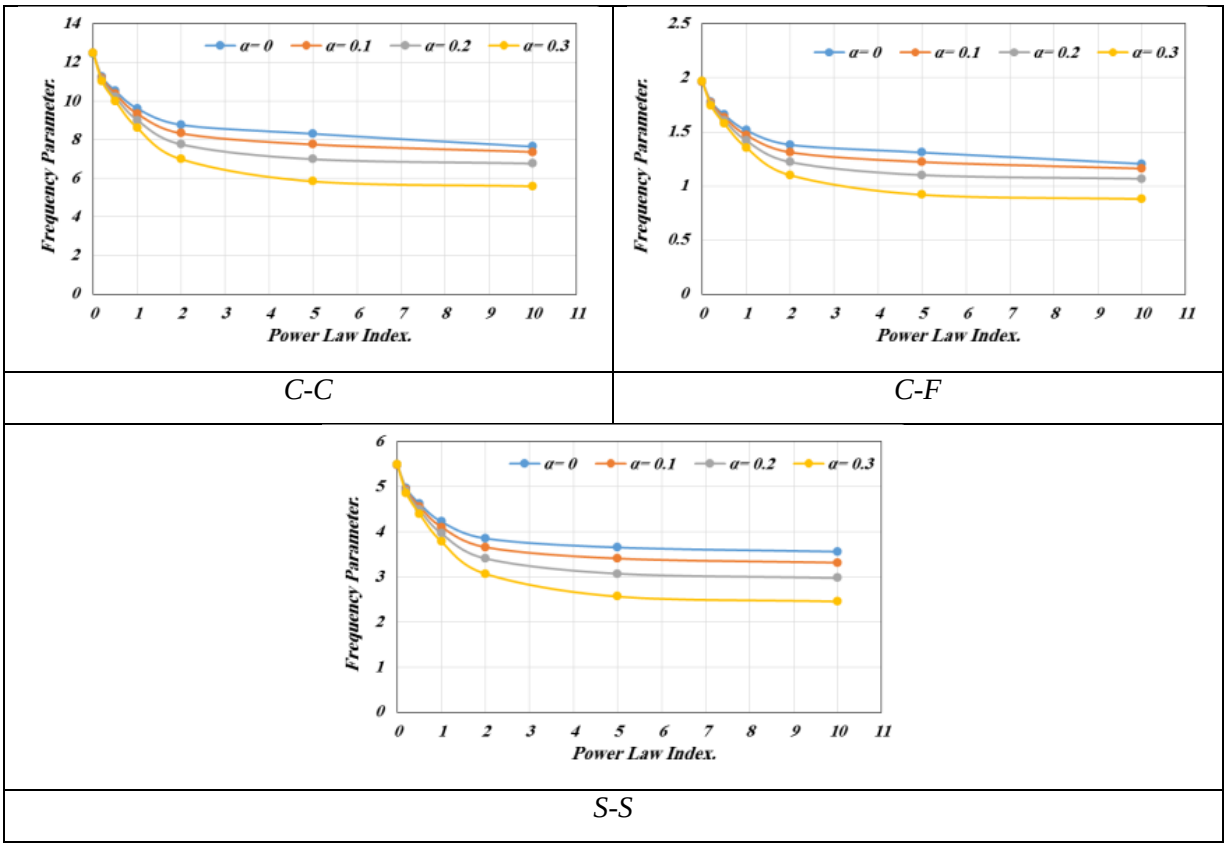

Figure 16. The Variation of the first natural frequency parameters of Uneven porous FG beam due to variation of power-law index (K) for different supporting types when L/h=40.

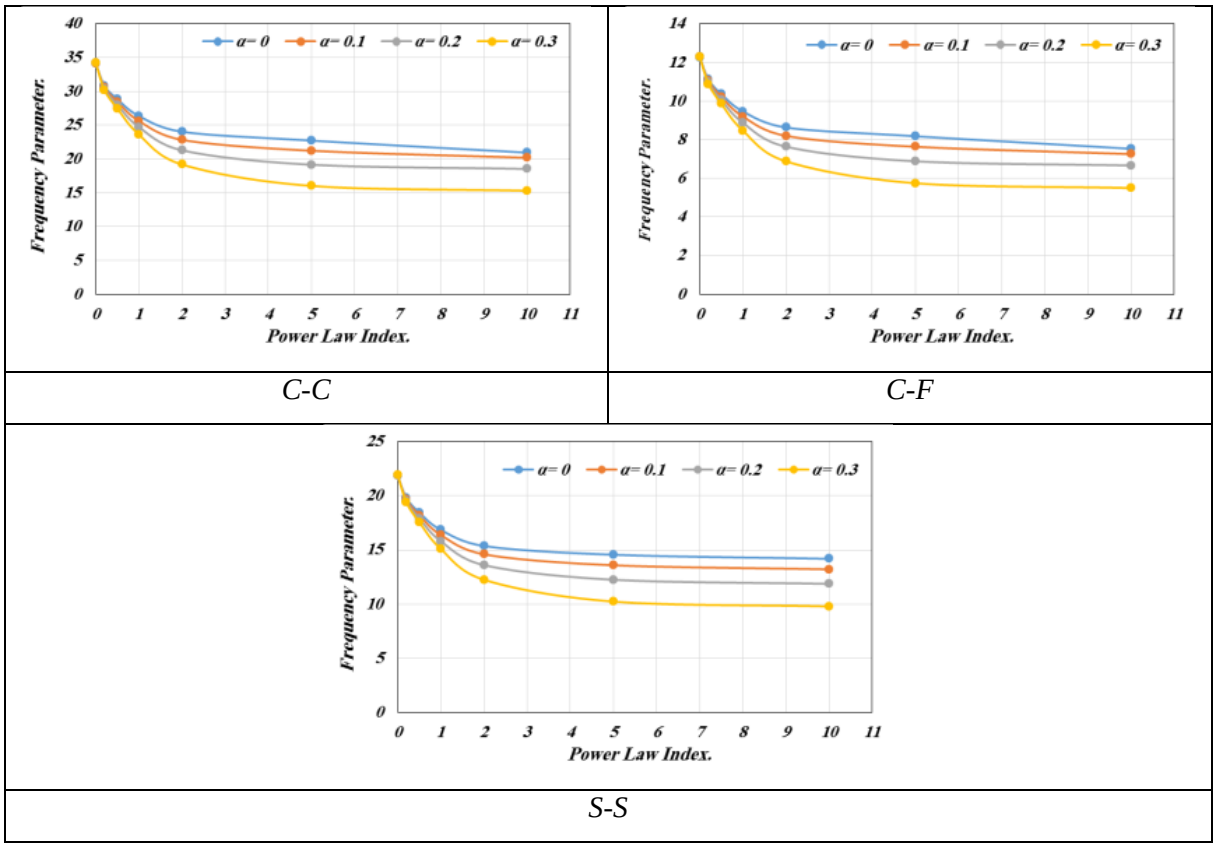

Figure 17. The Variation of the second natural frequency parameters of Uneven porous FG beam due to variation of power-law index (K) for different supporting types when L/h=40.

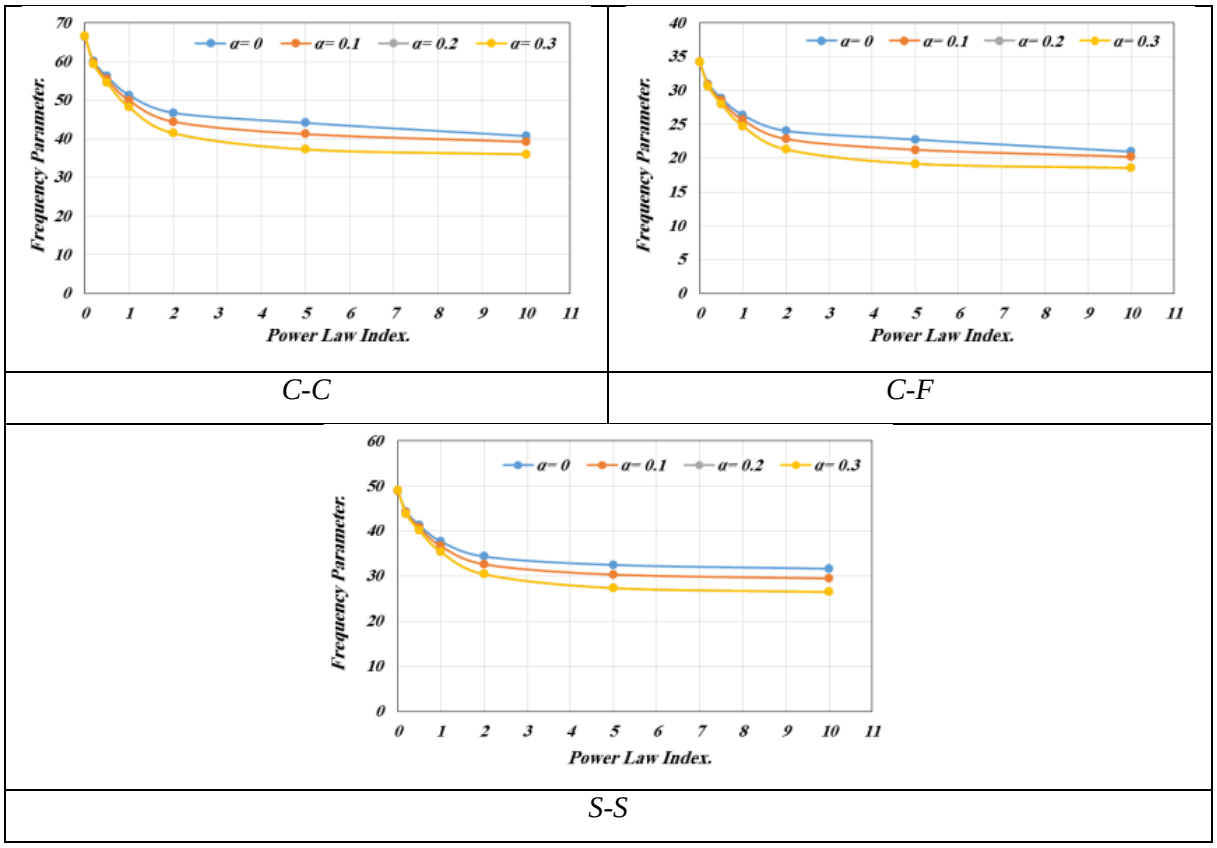

Figure 18. The Variation of the third natural frequency parameters of Uneven porous FG beam due to variation of power-law index (K) for different supporting types when L/h=40.

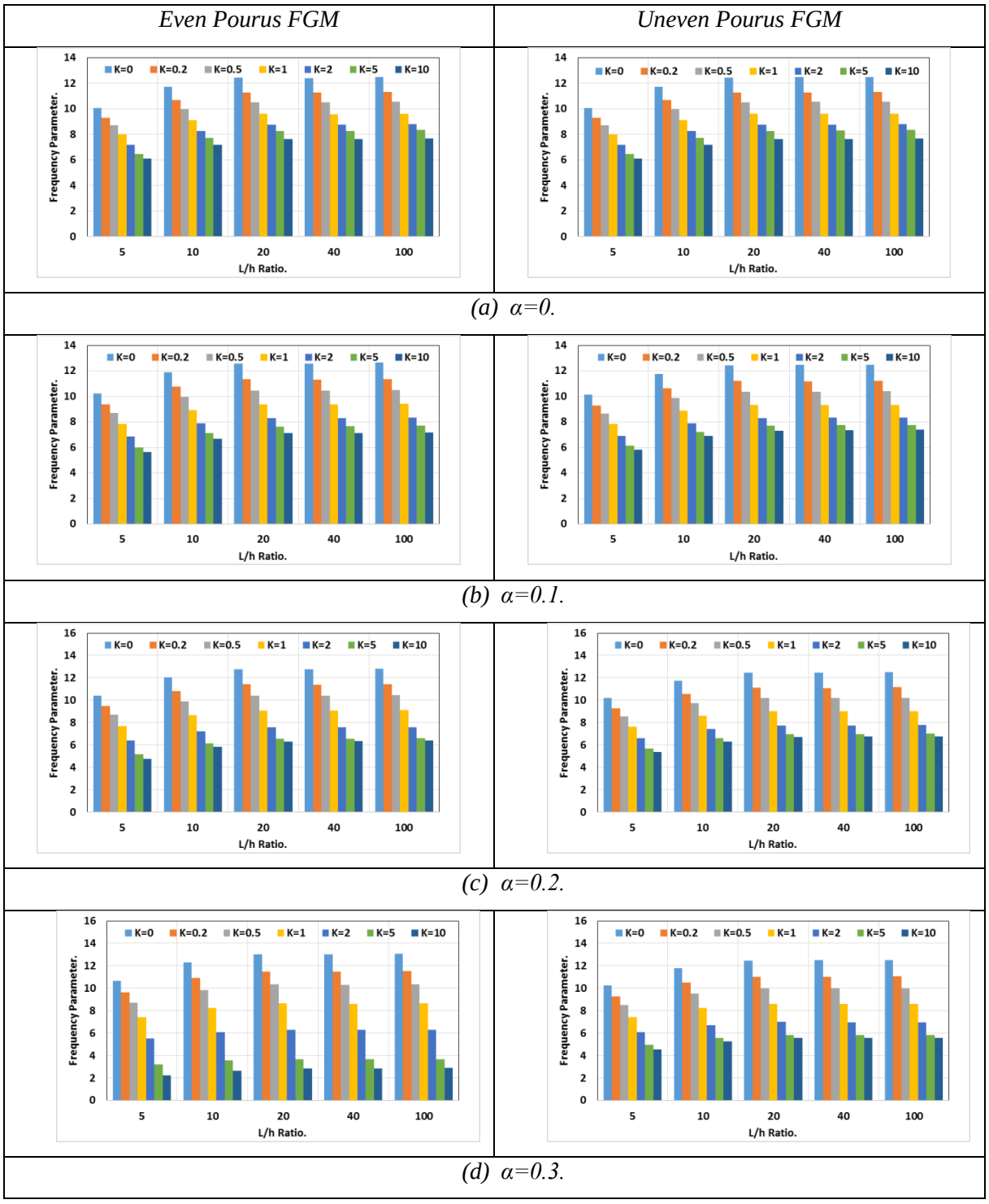

Figure 19. The impact of length.-to-.height ratio on the first natural frequency parameter of the even and uneven Clamped- Clamped porous FG beams for different power.-.law Index and porosity index.

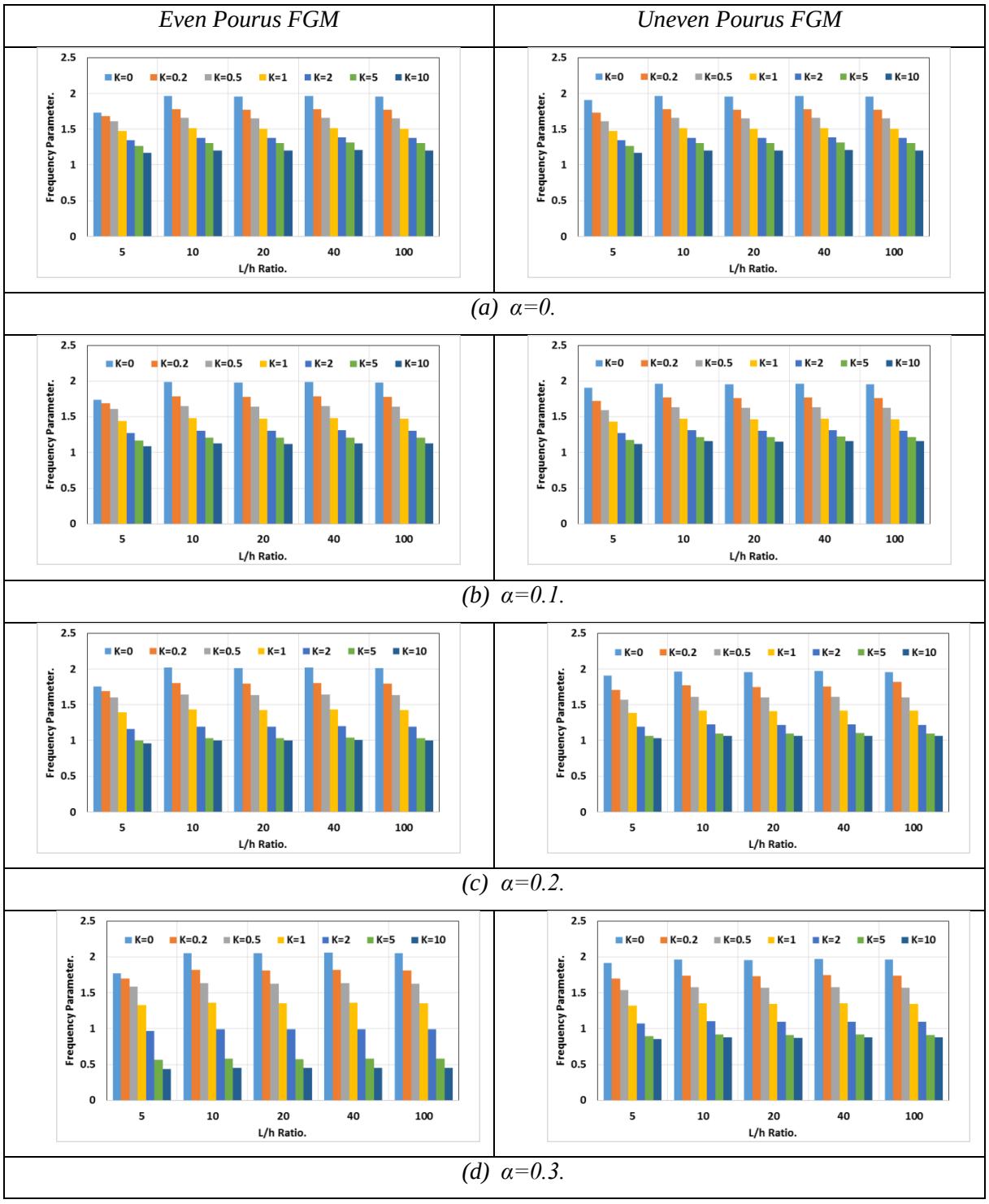

Figure 20. The impact of length.-to-.height ratio on the first natural frequency parameter of the even and uneven Clamped- Free porous FG beams for different power-law Index and porosity index.

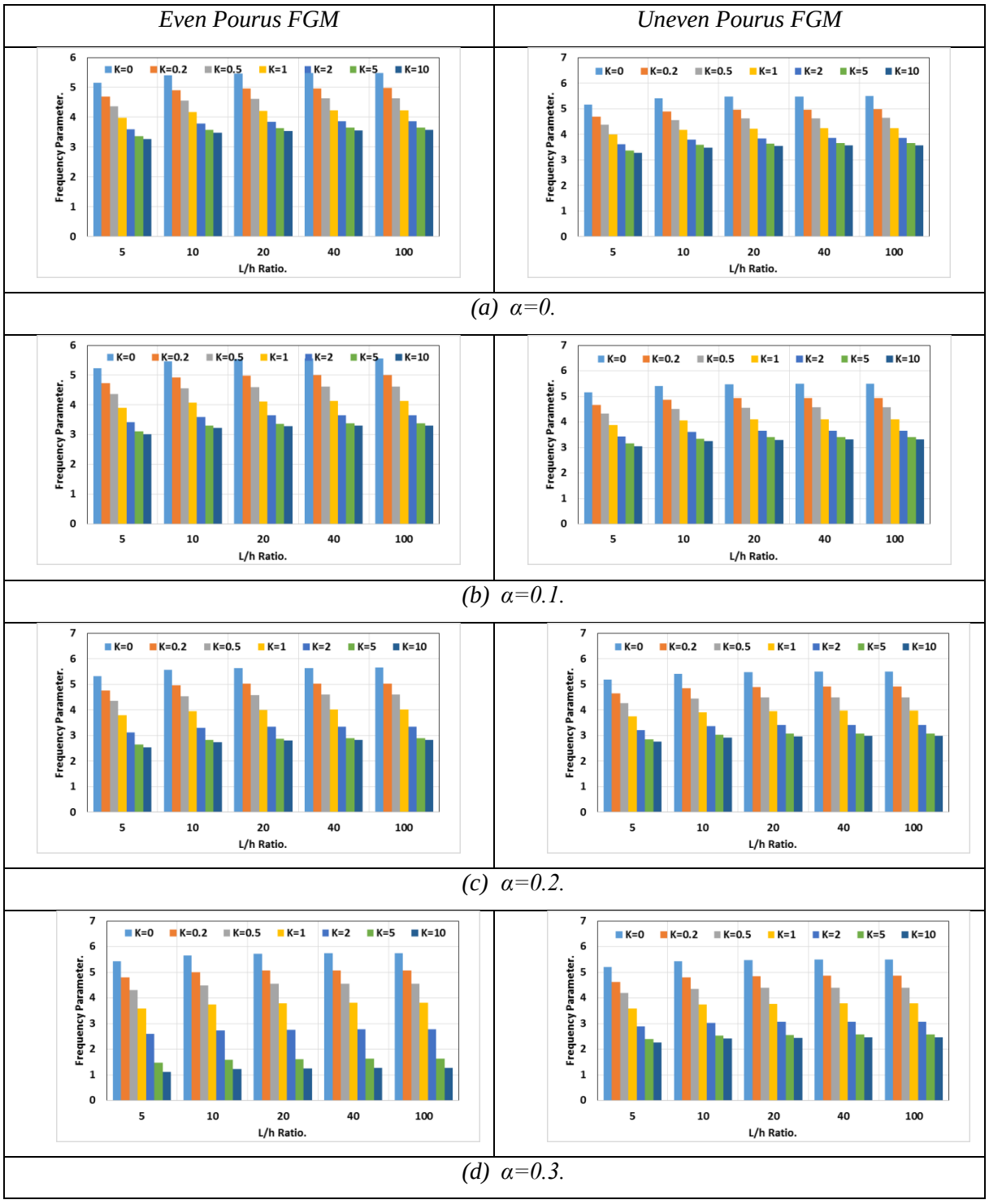

Figure 21. The impact of length-to-height ratio on the first natural frequency parameter of the even and uneven Simply supported porous FG beams for different power.-.law Index and porosity index.

5. Conclusions and Future Works

The first three natural frequencies of the porous FG beam, calculated using the finite element method and ANSYS APDL software, serve as a crucial frequency parameter. This parameter allows us to delve into the impacts of the power-law index, porosity index, porosity distribution function, length-to-height ratio, and supporting type on the first three natural frequency parameters. The power-law index, porosity index, porosity distribution function, length-to-height ratio, and supporting type are all key factors in our analysis. Based on earlier results, we can draw significant conclusions.

(1) The comparison between the frequencies results of the present model and that available in literatures shows a very good agreement between them and proves the accuracy of the present model.

(2) For even porous FG beam, the first three frequency parameters decrease when the power - law index (K) increases at any porosity index and any supporting types, while, When the porosity index increases, the frequency parameter decreases for any power- law and any supporting types.

(3) For an uneven porous FG beam, the first three frequency parameters decrease when the porosity index increases at any power index and any supporting types. On the other side, the effect of the power-law index on the natural frequency parameters appears sharply and takes the same profile in the first, second, and third natural frequencies.

(4) The impact of the length-to-height ratio on the frequency parameters vanishes when the length-to-height ratio is equal to or larger than (20).

(5) The values of the frequency parameter increase with increasing the mode number for the same power index, porosity index, porosity distribution function, length-to-height ratio, and supporting number.

The present work marks a significant stride in the analysis of the dynamic response of the porous FG beam under various supporting conditions. In our future endeavors, we aim to delve deeper into the harmonic and transient vibration behaviors, calculated by ANSYS APDL, to further understand the impacts of power-law index, porosity index, porosity distribution function, length-to-height ratio, and supporting type on the dynamic response.

References

[1] Gökhan Adıyaman (2022). Free vibration analysis of a porous functionally graded beam using higher-order shear deformation theory. Journal of Structural Engineering & Applied Mechanics (2022) 5(4): 277-288.DOI 10.31462/jseam.2022.04277288

[2] C. Y. Huang, Y. L. Chen, Effect of mechanical properties on the ballistic resistance capability of Al2O3-ZrO2 functionally graded materials, Ceramics International, 42(11), 2016, 12946-12955 Doi: 10.1016/j.ceramint.2016.05.067.

[3] M. Naebe, K. Shirvanimoghaddam, functionally graded materials: A review of fabrication and properties, Applied Materials Today, 5, 2016, 223-245 Doi: 10.1016/j.apmt.2016.10.001.

[4] G. Udupa, S. S. Rao, K. V. Gangadharan, Functionally Graded Composite Materials: An Overview, Procedia Materials Science, 5, 2014, 1291-1299 https://doi.org/10.1016/j.mspro.2014.07.442.

[5] V Lan Hoang That Ton (2022). Effect of porosity on free vibration of functionally graded porous beam based on simple beam theory. Technical Journal of Daukeyev University. Volume 2, Issue 1, 2022, pp. 1-10. DOI: https://doi.org/10.52542/tjdu.2.1.1-10

[6] H. L. Ton-That, H. Nguyen-Van, T. Chau-Dinh, A novel quadrilateral element for analysis of functionally graded porous plates/shells reinforced by graphene platelets, Archive of Applied Mechanics, 91(6), 2021, 2435-2466 Doi: 10.1007/s00419-021-01893-6.

[7] T. T. Hoang Lan, A Combined Strain Element to Functionally Graded Structures in Thermal Environment, Acta Polytechnica, 60(6), 2020, 528-539 https://doi.org/10.14311/AP.2020.60.0528.

[8] S. P. Parida, P. C. Jena, R. R. Dash, FGM Beam analysis in Dynamical and Thermal surroundings using Finite Element Method, Materials Today: Proceedings, 18, 2019, 3676-3682 https://doi.org/10.1016/j.matpr.2019.07.301.

[9] Y. Chen, G. Jin, C. Zhang, T. Ye, Y. Xue, Thermal vibration of FGM beams with general boundary conditions using a higher-order shear deformation theory, Composites Part B: Engineering, 153, 2018, 376-386 https://doi.org/10.1016/j.compositesb.2018.08.111.

[10] H. L. Ton-that, H. Nguyen-van, T. Chau-dinh, Static and buckling analyses of stiffened plate/shell structures using the quadrilateral element SQ4C, Comptes Rendus. Mécanique, 348(4), 2020, 285-305 https://doi.org/10.5802/crmeca.7.

[11] F. Ebrahimi, E. Salari, Thermal buckling and free vibration analysis of size dependent Timoshenko FG nanobeams in thermal environments, Composite Structures, 128, 2015, 363-380 https://doi.org/10.1016/j.compstruct.2015.03.023.

[12] H. L. Ton-That, The Linear and Nonlinear Bending Analyses of Functionally Graded Carbon Nanotube-Reinforced Composite Plates Based on the Novel Four-Node Quadrilateral Element,

European Journal of Computational Mechanics, 29(1), 2020, 139-172 https://doi.org/10.13052/ejcm2642-2085.2915.

[13] T. T. Hoang Lan, H. Nguyen-Van, A Combined Strain Element in Static, Frequency and Buckling Analyses of Laminated Composite Plates and Shells, Periodica Polytechnica Civil Engineering, 65(1), 2021, 56-71 https://doi.org/10.3311/PPci.16809.

[14] D. Chen, J. Yang and S. Kitipornchai (2015). Elastic buckling and static bending of shear deformable functionally graded porous beam. Composite Structures.Volume 133, 1 December 2015, Pages 54-61. http://dx.doi.org/10.1016/j.compstruct.2015.07.052

[15] Nuttawit Wattanasakulpong and Arisara Chaikittiratana (2015). Flexural vibration of imperfect functionally graded beams based on Timoshenko beam theory: Chebyshev collocation method. Meccanica. DOI 10.1007/s11012-014-0094-8

[16] Yousef S. Al Rjoub and Azhar G. Hamad (2016). Free Vibration of Functionally Euler-Bernoulli and Timoshenko Graded Porous Beams using the Transfer Matrix Method. KSCE Journal of Civil Engineering 21, pages792–806 (2017). DOI 10.1007/s12205-016-0149-6

[17] M.R. Galeban, A. Mojahedin, Y. Taghavi and M. Jabbari (2016). Free vibration of functionally graded thin beams made of saturated porous materials. Steel and Composite Structures, Vol. 21, No. 5 (2016) 999-1016.DOI: http://dx.doi.org/10.12989/scs.2016.21.5.999

[18] Noha Fouda, Tawfik El-midany and A.M. Sadoun (2017). Bending, Buckling and Vibration of a Functionally Graded Porous Beam Using Finite Elements. J. Appl. Comput. Mech., 3(4) (2017) 274-282. DOI: 10.22055/JACM.2017.21924.1121

[19] Şeref Doğuşcan Akbaş (2018). Forced vibration analysis of functionally graded porous deep beams. Composite Structures 186 (2018) 293–302. https://doi.org/10.1016/j.compstruct.2017.12.013.

[20] Saeed Amir, Zeinab Soleimani-Javid and Ehsan Arshid(2019). Size-dependent free vibration of sandwich micro beam with porous core subjected to thermal load based on SSDBT. Z Angew Math Mech. 2019; e201800334. https://doi.org/10.1002/zamm.201800334

[21] Ali Akbar Pasha Zanoosi (2020). Size-dependent thermo-mechanical free vibration analysis of functionally graded porous microbeams based on modified strain gradient theory. Journal of the Brazilian Society of Mechanical Sciences and Engineering (2020) 42:236. https://doi.org/10.1007/s40430-020-02340-3

[22] Souhir Zghal , Dhia Ataoui, and Fakhreddine Dammak (2020). Static bending analysis of beams made of functionally graded porous materials. MECHANICS BASED DESIGN OF STRUCTURES AND MACHINES. https://doi.org/10.1080/15397734.2020.1748053

[23] Farshad Rahmani, Reza Kamgar and Reza Rahgozar (2020). Finite Element Analysis of Functionally Graded Beams using Different Beam Theories. Civil Engineering Journal.Vol. 6, No. 11, November, 2020 http://dx.doi.org/10.28991/cej-2020-03091604.

[24] Armagan Karamanli and Thuc P. Vo (2020). A quasi-3D theory for functionally graded porous microbeams based on the modified strain gradient theory. Composite Structures.Volume 257, 1 February 2021, 113066. https://doi.org/10.1016/j.compstruct.2020.113066

[25] Mohsen Rahmani. (2021). Temperature-dependent Vibration Analysis of Clamped-free Sandwich Beams with Porous FG Core. Journal of Modern Processes in Manufacturing and Production, Volume 10, No. 4, Autumn 2021. DOR: 20.1001.1.27170314.2021.10.4.5.0

[26] B. Anirudh, M. Ganapathi, C. Anant and O. Polit (2021). A comprehensive analysis of porous graphene-reinforced curved beams by finite element approach using higher-order structural theory: Bending, vibration and buckling. Composite Structures.Volume 222, 15 August 2019, 110899. https://doi.org/10.1016/j.compstruct.2019.110899

[27] Ngoc-Duong Nguyen, Thien-Nhan Nguyen, Trung-Kien Nguyen and Thuc P. Vo (2022). A new two-variable shear deformation theory for bending, free vibration and buckling analysis of functionally graded porous beams. Composite Structures 282 (2022) 115095. https://doi.org/10.1016/j.compstruct.2021.115095

[28] Muhittin Turan, Ecren Uzun Yaylac and Murat Yaylac (2023). Free vibration and buckling of functionally graded porous beams using analytical, finite element, and artificial neural network methods. Archive of Applied Mechanics (2023) 93:1351–1372. https://doi.org/10.1007/s00419-022-02332-w

[29] Raghad Azeez Neamah , Ameen Ahmad Nassar and Luay S. Alansari . Modeling and Analyzing the Free Vibration of Simply Supported Functionally Graded Beam. J. Aerosp. Technol. Manag., São José dos Campos, v14, e1522, 2022. https://www.jatm.com.br/jatm/article/view/1264/938

[30] Zainab Abbood & Luay S. AlAnsari. Calculating the fundamental frequency of power law functionally graded beam using ANSYS software . IOP Conference Series: Materials Science and Engineering, Volume 1090, 1st International Conference on Engineering Science and

Technology (ICEST 2020) 23rd-24th December 2020, Samawah, Iraq; doi:10.1088/1757-899X/1090/1/012014; https://iopscience.iop.org/article/10.1088/1757-899X/1090/1/012014

[31] Help of ANSYS APDL Software Version 17.2.

[32] Kahya V, Turan M (2017) Finite element model for vibration and buckling of functionally graded beams based on the first-order shear deformation theory. Composites Part B: Engineering 109:108-115. https://doi.org/10.1016/ j. compositesb.2016.10.039.

[33] Nguyen T-K, Truong-Phong Nguyen T, Vo TP, Thai H-T (2015) Vibration and buckling analysis of functionally graded sandwich beams by a new higher-order shear deformation theory. Composites Part B: Engineering 76:273-285. https://doi.org/10.1016/j.compositesb.2015.02.032

[34] Vo TP, Thai H-T, Nguyen T-K, Maheri A, Lee J (2014) Finite element model for vibration and buckling of functionally graded sandwich beams based on a refined shear deformation theory. Engineering Structures 64:12-22. https://doi.org/10.1016/j.engstruct.2014.01.029.

[35] Mohammed A. Jebur and Luay S. Alansari "Free Vibration Analysis of Non-Prismatic Beam under Clamped and Simply Supported Boundary Conditions" Mathematical Modelling of Engineering Problems Vol. 10, No. 5, October, 2023, pp. 1630-1642. https://doi.org/10.18280/mmep.100513.

حساب التردد الطبيعي لعتبة مسامية متدرجة وظيفيا

الخلاصة :دراسة الاهتزاز الحر لعتبة مسامية متدرجة وظيفيا (FG) بإتجاه الارتفاع(h) باستخدام نظرية تشوه القص من الدرجة الأولى وتحت الظروف الحدية (المثبتة - المثبتة، المثبتة -الحرة والمسند البسيط للطرفين). يتم وصف خصائص المواد بواسطة نموذج قانون القوى. تتكون المواد المستخدمة في الحالة النموذجية للشعاع المتدرج وظيفيًا (FG) من الألومنيوم (AL) والألومينا (AL_2O_3). تم النظر في نوعين من وظائف توزيع المسامية (المتساوية وغير المتساوية). تم تطبيق نموذج العناصر المحددة باستخدام برنامج ANSYS APDL الإصدار 17.2 واستخدام العنصر "SHELL281" لحساب الترددات الطبيعية وإظهار تأثيرات نسبة الطول إلى الارتفاع (L/h)، مؤشر قانون الطاقة (k)، توزيع المسامية ومؤشرالمسامية (α). تم تقييم النتائج العددية مع بعض الأبحاث السابقة لدراسة تأثير دالة توزيع المسامية، ومؤشر قانون الطاقة، ومؤشر المسامية، وأنواع المساند لقيم الترددات الثلاثة الأولى اللأبعدية لحزمة FG. وتمت مقارنة نتائج النموذج الحالي مع البحوث السابقة مما يدل على اتفاق جيد. بالنسبة لحزم FG المسامية، مع ارتفاع مؤشر قانون الطاقة (k) يقلل من قيم الترددات الثلاثة الأولى، في حين أن زيادة مؤشر المسامية يقلل من قيم التردد. لوحظ تأثير مؤشر قانون الطاقة ومؤشر المسامية في عوارض FG غير المسامية وان نسبة الطول إلى الارتفاع لها تأثير ضئيل.

الكلمات المفتاحية:العتبة المسامية , التردد الطبيعي , عتبة متدرجة وظيفيا , نموذج قانون القوة , برنامج , ANSYSطريقة العناصر المحددة.